We are IntechOpen, the world's leading publisher of Open Access books Built by scientists, for scientists

6,900
Open access books available

185,000
International authors and editors

200M
Downloads

154
Countries delivered to

Our authors are among the

TOP 1%
most cited scientists

12.2%
Contributors from top 500 universities

CLARIVATE ANALYTICS
BOOK CITATION INDEX
INDEXED

WEB OF SCIENCE™

Selection of our books indexed in the Book Citation Index
in Web of Science™ Core Collection (BKCI)

Interested in publishing with us?
Contact book.department@intechopen.com

Numbers displayed above are based on latest data collected.
For more information visit www.intechopen.com

Thermodynamics and Mesomechanics of Nanostructural Transitions in Biological Membranes as Liquid Crystals

Lev Panin

Scientific Research Institute of Biochemistry SB RAMS
Russia

1. Introduction

Biological membranes play a key role in structural-functional organization of any cells. Membranes constitute 65% of the cell dry weight, of them 40% belong to lipids and 60% to simple and conjugate proteins. Membranes separate cell into functional units (divisions); as a result, cell operates as a complicated factory in miniature. Besides, membranes integrate the operation of cell as a whole. Cell is an open system. It steadily exchanges weight, energy and information with the environment. This process also involves the biological (cell) membranes.

All biological membranes are liquid-crystalline structures. They consist of phospholipids bilayer, with simple and conjugate proteins immersed in it. These are various membrane-bound enzymes, transmembrane carriers (of glucose, Na^+ and K^+ ions, and others), and hormone receptors that serve as signal mechanisms of the cell.

Structure-forming bonds in liquid crystals are represented by covalent and hydrogen bonds, hydrophobic and electrostatic interactions. These are the low-energy binding: covalent bonds — 50-100 kcal/mol, hydrogen bonds — about 6 kcal/mol.

Between fatty acid tails of phospholipids there is a large amount of water dipoles. Such structure of the membrane provides high mobility of its structural components relative to each other. Membranes are reinforced by cholesterol molecules, which strengthen the hydrophobic interactions.

Such membrane responds to external action as a cooperative system.

2. Changes in structure and function of erythrocyte membranes in vivo

These studies were performed with thirteen participants of a Russia-Canadian transarctic ski transition "Dickson (Russia) - North Pole - Canada" within the polar day period (Observation…, 1992). In this section, we present the results of analysis of the structural-functional characteristics of erythrocyte membranes within a long (three-month) stay of humans in arctic deserts.

2.1 Methodology

Erythrocyte 'shadows' were obtained at Dickson, the North Pole, and in Ottawa. The objectives of this investigation were to study the viscosity, specific electrical conductivity,

and the activation energy associated with ionic transport, to analyze the structure of the cell membrane by infrared spectroscopy, and to determine K_m and V_{max} for the Na^+, K^+ -ATPase. Observations were made over the temperature range 34-42 °C.

Viscosity and electrical conductivity were plotted against temperature, and the points of phase transition (Tc) were determined for each sample. A shift in phase transition reflects structural and functional changes in the membrane, with implications for Na^+, K^+-ATPase. The activity of this membrane-bound enzyme depends strongly upon the degree of order in the membrane (that is, upon the content of polyenoic fatty acids and cholesterol, the type of phospholipids, the presence of their lysoforms and structural transitions).

The viscosity was measured in an ultrathermostat, by traditional capillary viscosimetry. The speed of flow of a suspension of erythrocyte shadows through a capillary tube of known diameter (0.34 mm) and length (100 mm) was determined under a standard driving pressure (20 mm H_2O). Viscosity was measured at intervals of 1 °C over the 34-42 °C range, calculations being based on the equation:

$$P_x = P_o \, t_x \, / \, t_o \tag{1}$$

where P_o and P_x are the viscosities of the phosphate buffer and the suspension of erythrocyte shadows respectively, and t_x and t_o are the times for a fixed volume of the fluid (0.1 ml) to pass through the tube. Over the chosen temperature range, the viscosity of the buffer was 1 cP. The viscosity of the erythrocyte shadows was estimated to within 1 % relative to this standard.

The electrical conductivity of a colloidal solution depends on the disperse and the dispersive phases of the system (the number and motility of the colloidal particles, the size of their charge, and the number and charge of the ions in solution.

The charge on the particles is given by:

$$Q = z \cdot e \cdot k \, (1 + x \cdot z) \tag{2}$$

where z is the size of the particle, e is the dielectric strength, к is the electrokinetic potential, and x is the thickness of the double electrical layer around a colloidal particle. The specific conductivity C is then given by:

$$C = Q \cdot v \cdot U_o \tag{3}$$

where v is the number of particles in 1 cm^3, as determined from the ratio:

$$v = 0.01/\{4\pi Z^3/3\} \tag{4}$$

The term 0.01 assumes that 1% of colloidal particles are in the solution. U_o is the cataphoretic mobility, determined from the expression:

$$U_o = e \cdot k / 6\pi P \tag{5}$$

where P is the viscosity of the solution. By substitution,

$$C = 0.01 \cdot e^2 \cdot k^2 \cdot (1 + x^2)/8\pi^2 \cdot Z^2 P \tag{6}$$

From this final equation, it emerges that the electrical conductivity of a colloidal system is strongly influenced by the particle's electrokinetic potential, the dielectric strength, the particle size, the thickness of the double layer and the viscosity of the solution. The

equations presented are strictly limited to particles around 50 Å in size, but the concepts can be extended to larger particles, provided that the concentration and surface potential of the colloid, and the concentrations of the potential-forming ions in solution are all low.

Biological membranes display some of the properties of liquid crystals. The temperature dependence of conductivity of the erythrocyte shadows should thus be given by the expression:

$$C = C_o \, e^{-Ea/KT} \tag{7}$$

where C_o is a constant depending on the nature of the particle, K is Boltzmann's constant, Ea is the activation energy, and T is the absolute temperature. The temperature dependence should also be related to the number and motility of the carriers of current, according to the equation:

$$C = n \cdot e \cdot m_o \tag{8}$$

where n is the number of free charges, m_o is the motility of the charge, and e is the charge on an electron.

The experimental technique measured the resistance of suspensions of erythrocyte shadows when these were placed in a cuvette with electrodes of known surface, separated by a known distance. A 6-V, 2-kHz voltage was applied. Conductivity was then obtained as the inverse of specific resistance. The concentration of the shadows was 0.46 mg/ml, measured as a protein concentration, while the dispersing sodium/potassium/phosphate buffer had a pH of 7.4 and an osmolality of 310 osm.

Structural changes in the erythrocyte membrane were also evaluated by infrared spectroscopy. A suspension of the erythrocyte shadows (0.2 ml) was placed in a cuvette with a calcium fluoride base, and was vacuum dried for 1.0-1.5 h at 3-4 °C. The film of dried erythrocytes was then treated twice with phosphate buffer and was incubated at the desired temperature for 30 min before vacuum drying at 21-23 °C for a further 15 min. Spectra were determined on an(UR)-20 infrared spectrophotometer. Measurements were made of the half widths of absorption at 1660 cm^{-1} (corresponding to the C=O bonds in proteins), 1,000-1,100 cm^{-1} (the P – O – C bond in phospholipids), 1,500-1,700 cm^{-1} (C=O and NH bonds in proteins), and 2,700-3,000 cm^{-1} (the C−H bonds in proteins and phospholipids), together with the maximum intensity of absorption at 1,745 cm^{-1} (C=O bond in phospholipids) and the background intensity at 1,480 cm^{-1}.

Since the erythrocyte membrane contains many proteins, it was not possible to translate the spectral absorption into standard units of liters per mole per centimeter. Rather, the integral of the absorption peak was expressed as square centimeters per gram of erythrocyte shadow. An essentially equal total mass of erythrocytes was used for preparing test films at the three sites (Dickson, 0.50 ± 0.05, North Pole 0.49 ± 0.09, and Ottawa 0.41 ± 0.06mg).

The spectrophotometer was calibrated using a polystyrol film. The relative error of the absorption measurements was estimated at 1%.

2.2 Changes in viscosity during the ski trek

The initial viscosity of the erythrocyte "shadow" suspensions at a temperature of 34 °C was 1.85 cP. The viscosity decreased rather uniformly as temperature increased, both in Dickson and in Ottawa (fig. 1), but the curve had an anomalous region between 36 and 38 °C.

In Canada, the phase transition was displaced upwards, by 0.5 °C, and changes in viscosity of the erythrocyte shadows were more marked than in Dickson or at the North Pole (table 1). The

data thus suggest that an increase in rigidity of the erythrocyte membranes developed during the course of the trek, which reversed after completion of the mission. These changes can probably be attributed to increases in lysoforms phospholipids, and lipid hydroperoxides. Not only would such changes disturb hydrophobic interactions, making the membranes more porous, but they would presumably increase interactions between proteins and lipids, making the membrane more stable. Later, these changes may have been offset by an increase in the number of newly formed erythrocytes, giving the increased delta viscosity seen in Ottawa.
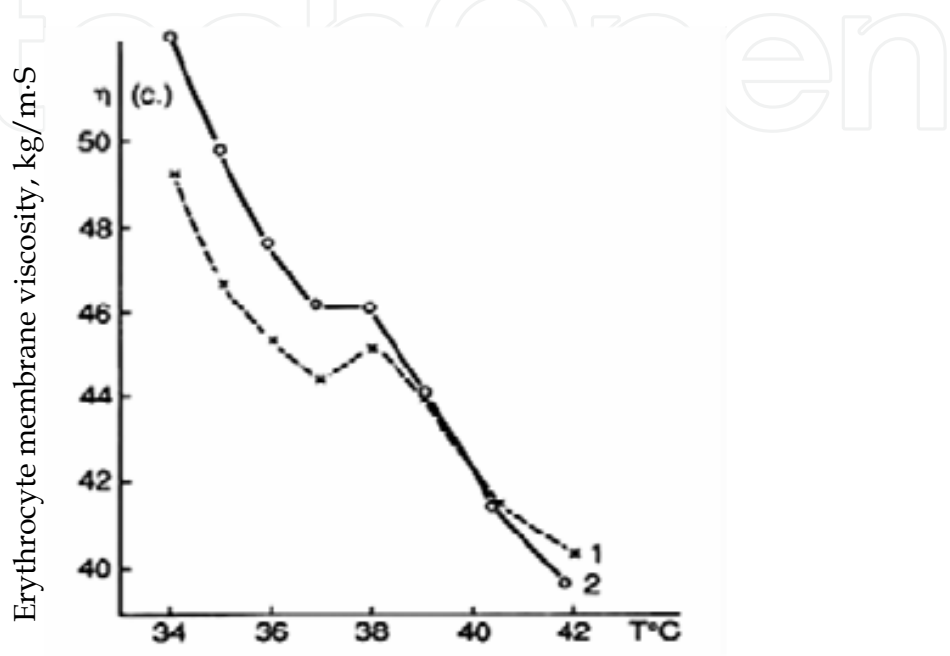
Fig. 1. Temperature dependence of viscosity of erythrocyte "shadows" on Dickson (1) and in Ottawa (2)

Parameters	Origin of the blood sample		
	Dickson	North Pole	Ottawa
Point of Phase transition, $^{\circ}$C	36.7±1.2	36.7±1.4	37.2±1.1
Viscosity Changes, kPa	0.305±0.063	0.220±0.091*	0.439±0.136*

Table 1. Changes in viscosity of erythrocyte 'shadows' over the temperature range 34-42 °C (mean ± SD)

*- Differences (p < 0,05) from Dickson

2.3 Changes in electrical conductivity during the ski trek

At low temperatures, conductivity showed an almost exponential relationship to temperature, but at high temperatures the relationship (fig. 2). became more linear. The transition from one pattern of temperature dependence to the other was smoother than that observed in homogenous liquid crystals (table 2).

The transition points showed no significant differences between the blood samples collected on Dickson, at the North Pole and in Ottawa. However, differences in activation energy before and after the phase transition point indicate the structural change in the cell membrane at 37-38 °C. Moreover, the ratios of activation energies at low and high

Thermodynamics and Mesomechanics of Nanostructural Transitions
in Biological Membranes as Liquid Cristals
319

temperatures changed over the trek, being highest at the North Pole. The increase in activation energy at the North Pole, and subsequently in Ottawa, suggests that the small ions (H^+, K^+, Na^+ etc) had less ability to compensate for their particulate charge in a suspension of membranes with a lesser structural integrity (table 3).

Parameters	Origin of the blood sample		
	Dickson	North Pole	Canada
Point of Phase transition, °C	37.5±1.2	37.7±1.0	36.7±1.0
Changes in intrinsic electrical conductivity, $\Omega^{-1} \times m^{-1}$	0.131±0.035	0.101±0.029*	0.105±0.022*

Table 2. Changes in the phase transition point and intrinsic electric conductivity of erythrocyte shadows over the temperature range 34-42 °C (mean ± SD)
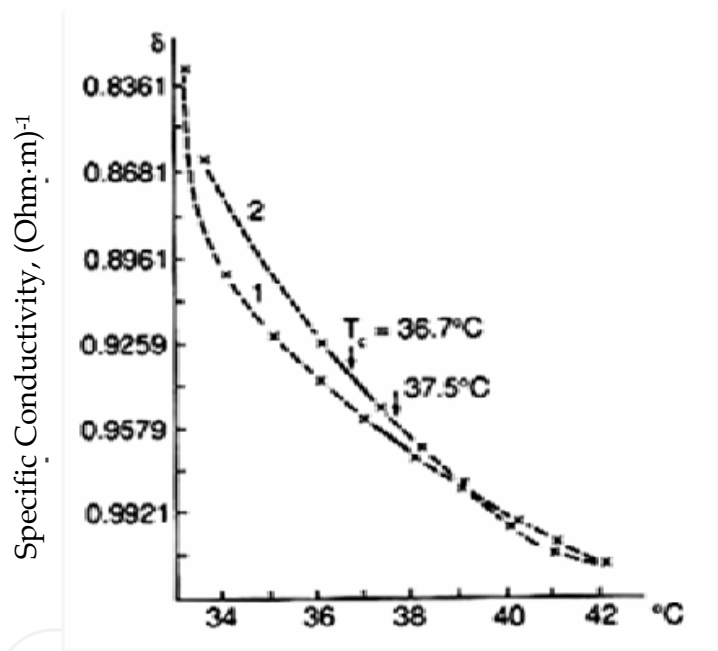* - *Differences (p < 0,05) from Dickson*

Fig. 2. Temperature dependence of electrical conductivity of erythrocyte "shadows" on Dickson (1) and in Ottawa (2)

Origin of the sample	Activation energy, cal/mg		
	Ea_1	Ea_2	Ea_1/Ea_2
Dickson	6.492 ± 2.487	5.106 ± 2.955	1.643 ± 0.475
North Pole	7.325 ± 2.707	3.148 ± 1.085	2.306 ± 1.051
Canada	11.771 ± 2.494	5.592 ± 2.045	2.108 ± 1.012

Table 3. Activation energy (Ea) of erythrocyte 'shadows' at low temperature (Ea_1) and high temperature (Ea_2) parts of the dependence curve (mean ± SD)

2.4 Changes in Infrared absorbance during the ski trek

Absorption in the regions of C=O bond (1.660 cm^{-1}) and the NH bond (1.550 cm^{-1}) decreased significantly as the temperature of the measurements was reduced, these changes being more marked in the initial blood samples from Dickson than in the final specimens taken in Ottawa. The Dickson specimens also showed a significant decrease in absorption at 1.645-1.650 cm^{-1}, and at 1.635, 1.685 and 1.696 cm^{-1} (fig. 3). The difference between the two locations again points to the development of structural changes in the proteins of the erythrocyte membrane.

As the measuring temperature was decreased, there was also a change in absorption at 1.070 cm^{-1}, reflecting changes in the P–O–C grouping of the phospholipids, the difference amounting to 9.8% at Dickson, 6.9% at the North Pole, and 7.9% in Canada (table 4). The P–O–C region showed two maxima, at 1.070 and 1.090 cm^{-1}, this being more marked in Dickson than in Ottawa. Thus, changes in phospholipids also seem to have developed over the course of the trek.

Origin of the sample	Absorption intensity, % ΔI between 40 and 37 ˚C		
	1.660 cm^{-1}	1.070 cm^{-1}	1.660 cm^{-1}/1.070 cm^{-1}
Dickson	8.87 ± 3.48	9.85 ± 3.67	1.82 ± 0.37
North Pole	7.52 ± 4.00	6.92 ± 2.31	2.61 ± 0.21
Canada	5.87 ± 3.12	7.91 ± 4.75	2.54 ± 0.36

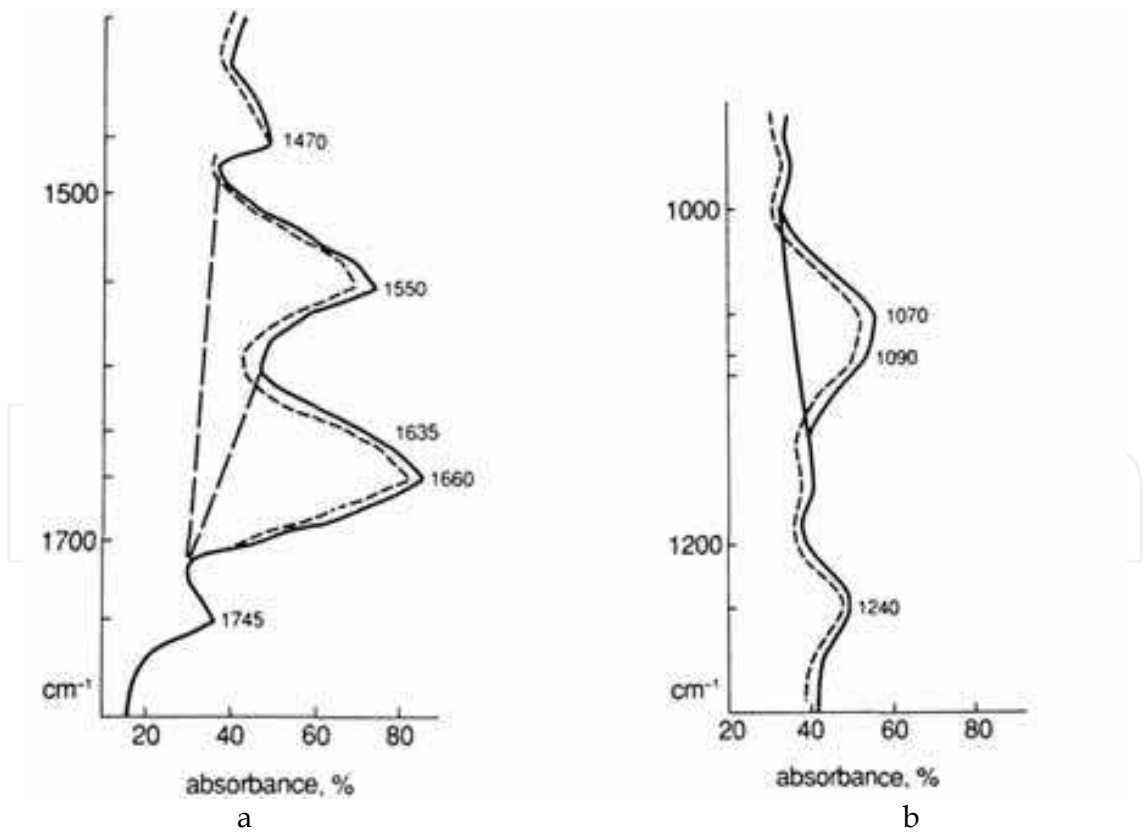Table 4. Temperature dependence of integrated intensity of the infrared spectra of erythrocyte "shadows" (mean ± SD)

Fig. 3. Infrared absorbance of erythrocyte shadows at Dickson, before trek: a. λ = 1400-1800 cm^{-1}, b. λ = 900-1300 cm^{-1}

———— 40 ˚C ; . _ _ _ _ 37 ˚C

Thermodynamics and Mesomechanics of Nanostructural Transitions
in Biological Membranes as Liquid Cristals
321

Disarrangement of the structural proteins was further suggested by an increase in absorption at the wavelength of the C=O bond 1.660 cm^{-1}. The decrease in absorption at 1.745 cm^{-1} points to a reduced phospholipids content of the membrane at the North Pole and in Canada, relative to the Dickson baseline (table 5).

The intensity of background absorbance at 1.480 cm^{-1} depends on the water content of the sample. Given the standard conditions of vacuum drying, any alteration of this value must reflect changes in the amount of bound water. Values were 10% higher at the North Pole (fig. 4) and in Canada (fig. 5), relative to initial blood samples. This suggests that there was an increase in the hydration of the proteins and/or phospholipids.
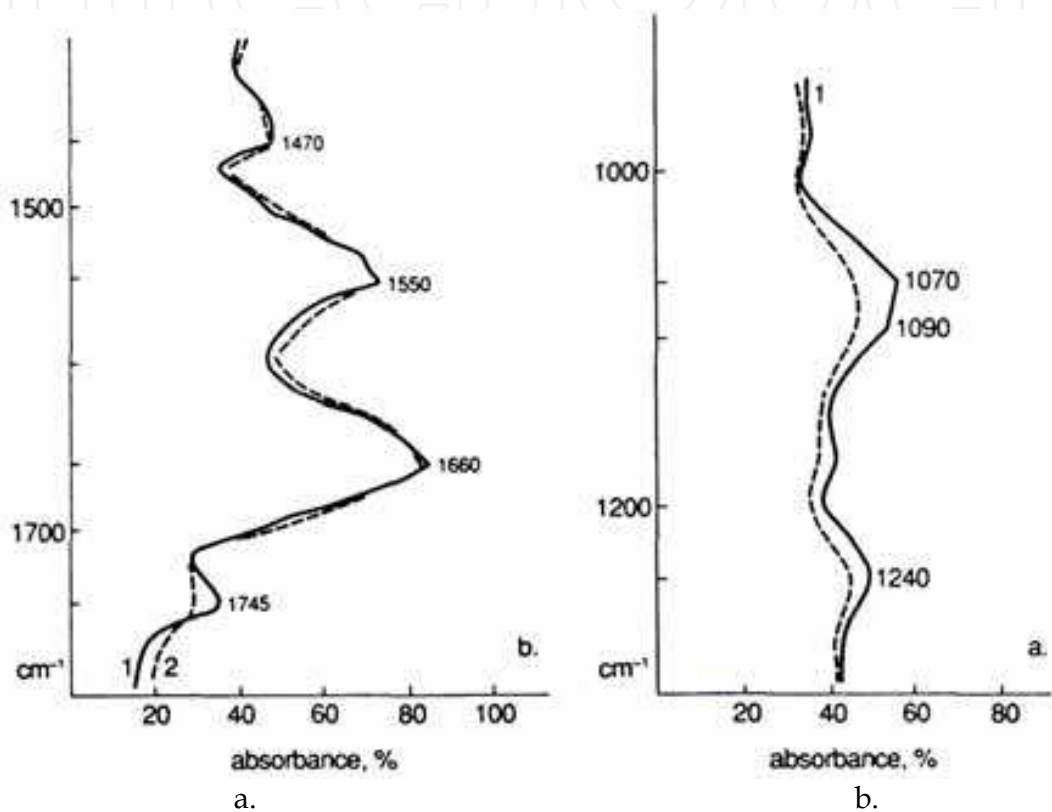

Fig. 4. Infrared absorbance of erythrocyte shadows at North Pole: a. λ = 1400-1800 cm^{-1}, b. λ = 900-1300 cm^{-1}.
———— 40 ˚C ; . _ _ _ _ 37 ˚C

Integrated absorbance over the range 2.700-3.000 cm^{-1} was increased at the North Pole and in Canada relative to the Dickson baseline. This reflects increased covalent CH bonding of fat and protein. There was an increase in splitting in the lipid parts of the spectrum (particularly, at 1.470 cm^{-1}), suggesting deformational oscillation of the CH bonds.

Origin of the sample	Absorption intensity, %		
	1.745 cm^{-1}	1.480 cm^{-1}	1.660 cm^{-1}
Dickson	18.9 ± 5.0	33.1 ± 8.8	64.2 ± 8.6
North Pole	15.5 ± 4.5	41.8 ± 8.0	82.4 ± 10.3
Canada	13.2 ± 3.8	40.9 ± 8.8	80.7 ± 9.5

Table 5. Changes in some characteristics of the infrared spectra of the erythrocyte "shadows" during the Ski trek (mean ± SD)

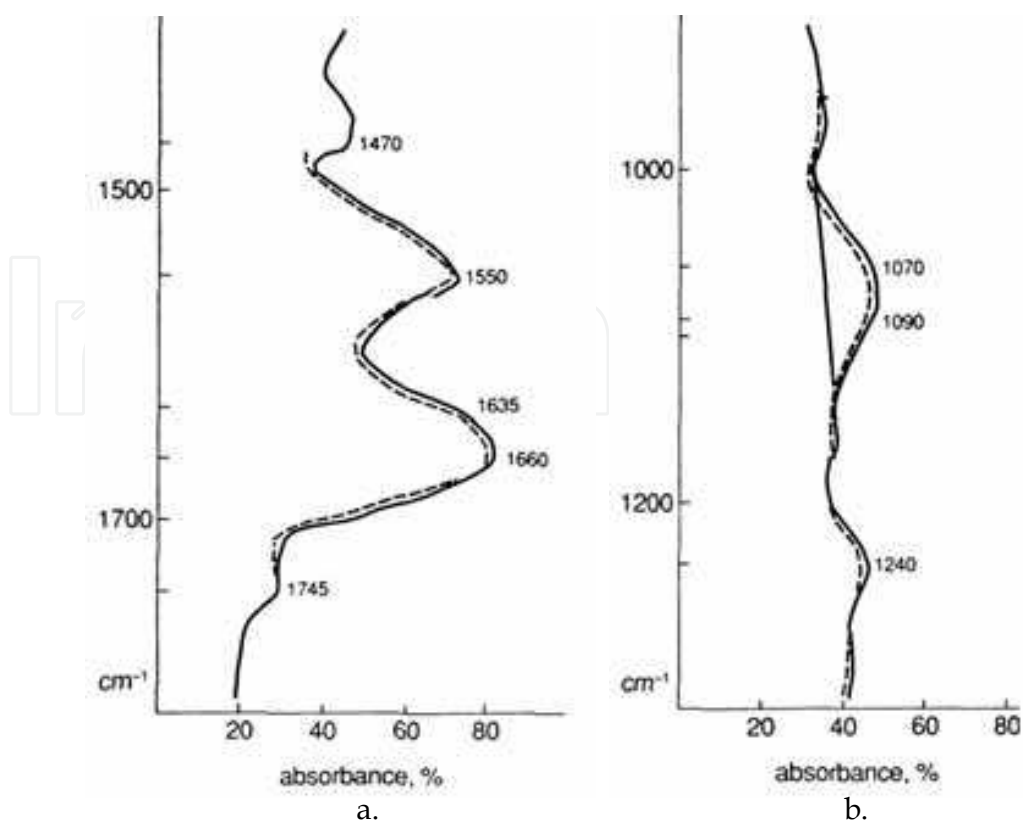Fig. 5. Infrared absorbance of erythrocyte shadows sampled in Canada after trek: a. λ = 1400-1800 cm⁻¹, b. λ = 900-1300 cm⁻¹
———— 40 ˚C ; . — — — — 37 ˚C

2.5 Changes in ATPase over the ski trek

The activity of ATPase and its K_m for ATP were both decreased in Ottawa relative to initial values in Dickson: from 3.50 ± 0.25 to 2.65 ± 0.32 mmol/mg/h, and from 5.64 ± 0.21 to 3.83 ± 0.72 mmol, respectively. Changes of kinetic characteristics of Na^+/K^+-ATPase of man erythrocyte "shadows' upon variation of suspension temperature are presented in table 6. In the North Pole the decrease in K_m was more then 30% in relation to Dickson. Thus, activity of Na^+/K^+-ATPase, which is responsible for maintaining the transmembrane electrochemical potential, decreased in 1.2-1.4 times. The Michaelis constant (Km), which determines the enzyme-substrate affinity, also decreased.

These changes could be related to a decreased content or an altered composition of phospholipids, together with conformational changes in the enzyme molecule itself. Probable, stress hormones (cortisol, adrenalin) also make a substantial contribution to the structural transitions. Their content in the blood serum was increased during the ski trek: cortisol before trek - 565±78 nmol/l, after trek - 927±70 nmol/l; adrenalin before trek – 0.7±0.03 mkg/l, after trek – 1.49±0.07 mkg/l.

2.6 Conclusions

Erythrocyte membranes responds to extreme conditions as cooperative system. The changes in intermolecular interactions and membrane permeability indicated by these various tests are not necessarily negative adjustments, since they enhance the rheological properties of the erythrocytes, and may also enhance the diffusion of oxygen through the cell membranes.

Thermodynamics and Mesomechanics of Nanostructural Transitions
in Biological Membranes as Liquid Cristals
323

However, when subjects are exercising hard, there may also be changes designed to modify the oxygen-transporting ability of the red cells, microviscosity of erythrocyte membranes etc.

Origin of the sample	T, ˚C	$K_m, M_{Atp} \cdot 10^{-6}$
Dickson	36	4.88 ± 0.54
	37	5.64 ± 0.21
	38	4.54 ± 0.11
North Pole	36	2.89 ± 0.13
	37	3.51 ± 0.34*
	38	2.92 ± 0.12
Ottawa	36	3.31 ± 0.15
	37	3.83 ± 0.72*
	38	3.61 ± 0.15

Table 6. Changes of Michaelis constant (Km) over the course of ski trek.
* - *Differences (p < 0,05) from Dickson.*

3. The interaction mechanism of cortisol and catecholamines with structural components of erythrocyte membranes

Physiological activity of the great majority of hormones is determined by the receptors located on plasmatic membranes of target cells. They all have high affinity for the hormone

cortisol

adrenaline

noradrenaline
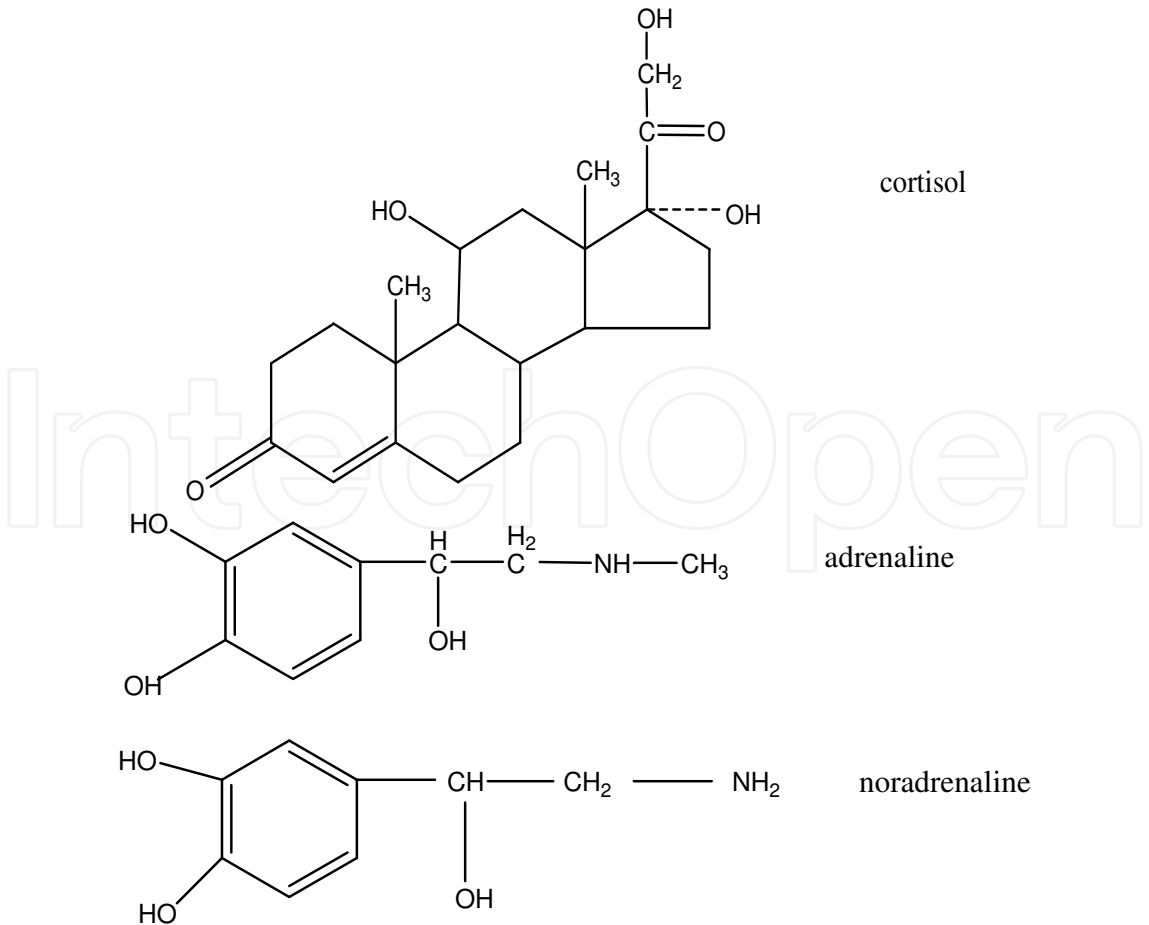
ligand. Detection of a rather large amount of steroid hormones in the albumin fraction of blood serum and on plasmatic membranes of some cells (erythrocytes, leukocytes) points to the possibility of their nonspecific (non-receptor) interaction with protein and membrane structures. Some mechanisms of this interaction are discussed in available literature (Sergeev et al., 1996). Here, of particular interest are glucocorticoids and catecholamines, which blood content may increase several fold under stress. This will increase nonspecific interaction of these hormones with plasmatic membranes of blood cells.

We studied cortisol and catecholamines interaction with erythrocyte membranes, and the mechanism of structural transitions that occur in membranes under the action of these hormones.

Three stress hormones: cortisol, adrenaline and noradrenaline (Amersham) is analyzed in the work.

3.1 Methodology
3.1.1 Atomic force microscopy (AFM) of erythrocytes

Erythrocytes were obtained from fresh blood after decapitation of Wistar rats under light nembutal narcosis. Blood was diluted twofold by isotonic phosphate buffer (pH 7.35) containing 0.16 M of KH_2PO_4 and 0.18 M of Na_2HPO_4. After precipitation of cells by centrifuging at 330 g for 10 min, supernatant liquor was decanted, and the washing procedure was repeated twice more.

All the procedures were performed at 4 °C. The resulting erythrocyte suspension of 20 mcl volume was deposited onto a glass slide as a thin smear. The smear was predried for 10 min in air at 24 °C and humidity of 40%. After evaporation of excessive surface moisture, the smear was observed under a «Solver Bio» atomic force microscope (NT-MDT, Russia) at 24 °C using a semi-contact mode. An analogous procedure of obtaining red blood cells for the AFM examination was employed earlier by other authors (Wu et al., 2009). In each experiment, we first tested a control specimen without hormones, and then the experimental one. Silicon cantilevers NSG11 (NT-MDT, Russia) with a resonant frequency between 120 and 180 kHz and spring constant ~ 6 N/m were used (all of these probe parameters were offered by manufacturer). Images of the surface relief of erythrocyte membrane after absorption of hormones were obtained with the scan size 1x1 μm^2 and 1.3x1.3 μm^2.

3.1.2 IR spectroscopy of erythrocyte shadows

Erythrocyte shadows were obtained after their hemolysis in hypotonic phosphate buffer (pH 7.35) containing 2.75 mM of KH_2PO_4 and 8.5 mM of Na_2HPO_4. Shadows were precipitated by centrifuging at 5500 g, supernatant liquor was decanted. The washing procedure was repeated four more times. All operations and further storage of shadows were performed at 4 °C.

A film for taking the IR spectra of erythrocyte shadows was prepared in a cuvette with fluorite backing via slow evaporation of water under weak vacuum at a pressure of ca. 0.1 atm (ca. $0.5 \cdot 10^4$ Pa) and temperature 4±1 °C (Kunitsyn et al., 2001). Drying lasted 180 min. A suspension of erythrocyte shadows in a 0.001 M phosphate buffer with pH 7.35 and volume 60 mcl was introduced into a cuvette. This was supplemented with 30 mcl of the same buffer and 1.0 mcl of the hormone solution with concentration 10^{-6} M. Stirring and incubation lasted 10 min at 16-17 °C. The cuvette was placed horizontally on a special table of a vacuum unit.

Thermodynamics and Mesomechanics of Nanostructural Transitions
in Biological Membranes as Liquid Cristals
325

When the film was prepared, the cuvette was transferred into an optical chamber and blown with dry air for 30 min, then the scanning unit was switched on. IR spectra were taken on a Specord-M80 spectrometer (Germany, Leipzig), sequentially experiment and control against the fluorite backing, or experiment and control to obtain a difference spectrum. Integration, determination of the spectrum band frequency, and mathematical processing were performed with special programs enclosed to the spectrometer.

3.1.3 Fluorescence analysis of erythrocyte shadows

Fluorescence measurements were performed with a Shimadzu spectrofluorophotometer RF-5301(PC)SCE. 4 ml of hypotonic phosphate buffer containing 2.75 mM of KH_2PO_4 and 8.5 mM of Na_2HPO_4 (pH 7.35), and erythrocyte shadows were poured into a quartz cuvette of size $1 \times 1 \times 4$ cm^3. The concentration of shadow proteins was determined by the Warburg–Christian method from changes in the optical density of suspension (Dawson et al., 1986). On the average, it varied in the range of 0.100-0.250 mg/ml.

A cuvette with the shadow suspension was placed into a spectrofluorimeter thermostat for 1 hour. Getting a stationary temperature regime in the cuvette was controlled by an electronic thermometer. In all the experiments, temperature in the cuvette was 36 °C. After establishing a stationary temperature in the cuvette, intensity of the intrinsic fluorescence of tryptophan residues in protein membranes was measured. The tryptophan emission spectrum was taken in the range of 300 nm $\leq \lambda \leq$ 400 nm at the excitation wavelength 281 nm, with the maximum of emission intensity observed at 332 nm. The average value of maximum emission intensity was obtained graphically after its continuous measuring for 4 minutes. Intensity of tryptophan fluorescence fluctuated within 1%. The possible reasons include variation of temperature in the cuvette with suspension, instrumental error in determination of fluorescence intensity, and photochemical reactions occurring in the system. Spectral width of the slits was 1.5/10. The tryptophan absorption spectrum was recorded in the range of 220 nm $\leq \lambda \leq$ 300 nm at the emission wavelength λ = 332 nm. Cortisol was dissolved in a mixture of dimethyl sulfoxide (DMS) and ethanol (1 : 1, V/V). Concentration of the hormone in the initial mother liquor was 10^{-3} M. If necessary, the solution was diluted with hypotonic phosphate buffer to obtain a desired concentration.

A solution of adrenaline or noradrenaline with the concentration 10^{-6} M was prepared in hypotonic phosphate buffer. The time of hormone incubation with shadows was one hour. Absorption and emission spectra were taken, the average value of emission and absorption intensity was measured. For each hormone (cortisol, adrenaline or noradrenaline), the binding constant K_b was calculated by the method (Attallah & Lata, 1968) as well as the stoichiometric concentration of a bound hormone B_{max} and a change in free energy of the system ΔG. The interaction of cortisol and erythrocyte membrane is described by the equation

$$B + nS = S_nB, \tag{9}$$

where B is a membrane protein, S is the hormone, and n is the number of moles of hormone per a mole of proteins. The binding constant K_b was calculated by the formula

$$K_b = [S_nB] / [S] \cdot [B] \tag{10}$$

where $[S_nB]$ is the concentration of bound protein, $[B]$ is the concentration of free protein, and $[S]$ is the concentration of free hormone. It is supposed that hormone, upon binding to

protein, completely quenches its fluorescence. Thus, the fluorescence intensity F will be proportional to the concentration of free protein. Let's write C for total concentration of protein in the cuvette, and x for concentration of the bound protein. Then,

$$F_{max} = \beta C; \qquad F = \beta (C - x) \qquad (11)$$

where F is the intensity of tryptophan fluorescence at $\lambda = 332$ nm (the excitation wavelength $\lambda = 228$ nm), F_{max} is the intensity of tryptophan fluorescence in the absence of hormone (when the entire protein is free), β is the proportionality factor, and A_s is the stoichiometric concentration of hormone. When concentration of hormone exceeds **A_s,** the fluorescence quenching does not increase. Dividing the first equation of set (11) by the second one gives

$$x = QC, \text{ where } Q = (F_{max} - F)/F_{max} \qquad (12)$$

$[S] = A - n \cdot x = A - n \cdot Q \cdot C$, where A is the total concentration of hormone; $n = A_s/C$; $[B] = C - x$ $= C(1-Q)$. Substitution of (11) and (12) into expression for binding constant (10) gives

$$K_b = Q / (1-Q)(A-nQC) \qquad (13)$$

In our case, molar mass of membrane proteins is unknown, so the concentration of proteins in cuvette C is determined in mg/ml, and concentration of hormones A in mol/l. The constant n is expressed in moles of molecules of hormone per milligram of protein (M/mg), and is a ratio of the maximum concentration of bound hormone to the concentration of membrane proteins. This can be written as

$$B_{max} = A_s/C \text{ [mole/mg protein]} \qquad (14)$$

Changes in Gibbs free energy ΔG of the system upon transition of hormone from aqueous medium to erythrocyte membrane are calculated by the formula

$$\Delta G = - RT \cdot \ln(K_c) \text{ [J/mole]}, \qquad (15)$$

where $R = 8,314$ J/K·mole, and T is the absolute thermodynamic temperature.

For adrenaline and noradrenaline, in formulas (11) and (12) we use the dependence of $Q_1 = (D_{max} - D)/D_{max}$ on concentration A of hormone introduced into the cuvette. Here, D_{max} and D are the intensities of tryptophan absorption in shadows at $\lambda = 228$ nm, respectively, without addition of hormone and with hormone. The emission wavelength $\lambda = 332$ nm.

The measurement errors appeared due to inaccuracy in volumetric dosing of the shadow suspension specimens and their titration against hormones. Specimens were dosed using pipette dispensers DPAOF-1000 and DPAOF-50, their relative error at (20±2)°C being 1% and 2%, respectively. 4 ml of the buffer was taken once with a DPAOF-1000 pipette, and suspension of erythrocytes and hormones was dosed twice using a DPAOF-50 pipette. The fluorescence intensity of erythrocyte shadows F is directly proportional to the concentrations of proteins C and hormones A in the specimen. Relative error E_F in measuring the F value can be estimated by the formula

$$E_F = \sqrt{(1\%)^2 + (2\%)^2 + (2\%)^2} = 3\% \qquad (16)$$

Relative measurement errors for K_b and B_{max} can be obtained in the same way. They are equal to 10%.

Thermodynamics and Mesomechanics of Nanostructural Transitions
in Biological Membranes as Liquid Cristals
327

In calculation, the values of fluorescence intensity F and absorption intensity D were corrected for dilution of suspension after the introduction of solution with hormone, for quenching of tryptophan emission by the solvent (a mixture of DMS and ethanol), for proper fluorescence of hormones, and evaporation of water from the cuvette.

3.1.4 Measurement of erythrocyte membrane microviscosity

Membrane microviscosity for translational diffusion of pyrene probe was calculated as a ratio of fluorescence intensity of the pyrene dimer to fluorescence intensity of the pyrene monomer (fig. 6). Microviscosity of erythrocyte membranes was measured also on a Shimadzu RF-5301(PC)SCE spectrofluorimeter. The experimental specimen was prepared as follows: 4 ml of hypotonic phosphate buffer containing 2.75 mM of KH_2PO_4 and 8.5 mM of Na_2HPO_4 (pH 7.35), a fluorescent pyrene probe, erythrocyte shadows and a specified amount of hormone were placed in a quartz cuvette of size $1 \times 1 \times 4$ cm^3. Before use, all the components were stored at 4 °C. The concentration of shadow protein in the cuvette was 0.100-0.250 mg/ml; that of pyrene, $7.76 \cdot 10^{-6}$ M. Pyrene was diluted in ethanol, its initial concentration being $1.5 \cdot 10^{-3}$ M. The cuvette was placed into the spectrofluorimeter thermostat for 10 min, then the fluorescence measurements were performed at 36 °C. Before placing the specimen into the spectrofluorimeter thermostat, it was shaken vigorously for 1 min. For fluorescence measurements of shadows upon their loading with a different amount of hormones, each time a new specimen was prepared by the same procedure. Such a procedure is necessary because pyrene favors fast degradation of erythrocyte membranes.
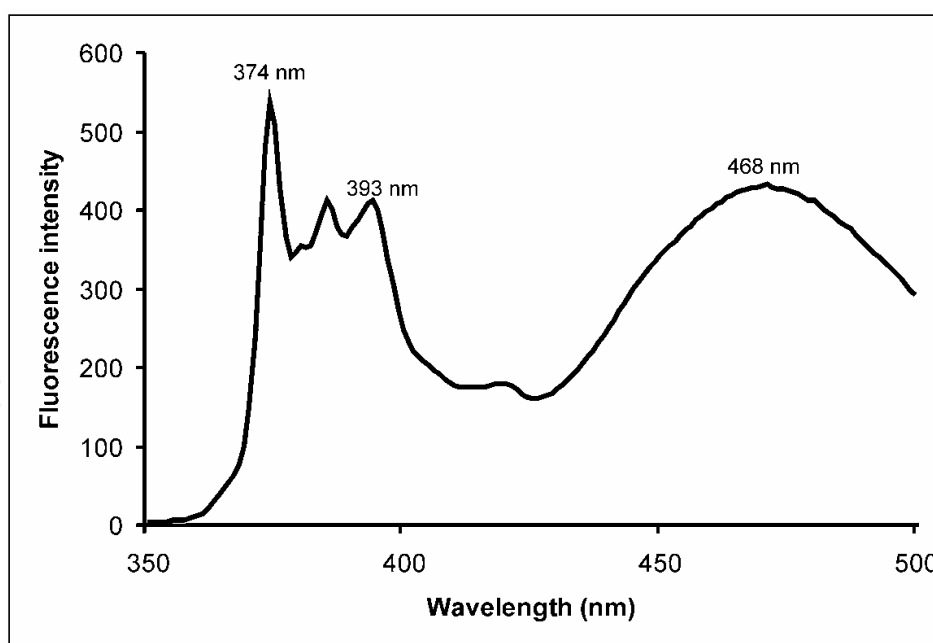

Fig. 6. Emission spectra of the pyrene in the suspension of shadows. Excitation wavelength $\lambda = 337$ nm and spectral slit width 1.5/3. At that, the maxima of emission intensity were observed at $\lambda = 374$ nm and $\lambda = 393$ nm (the vibronic emission peaks of excited pyrene monomers), and $\lambda = 468$ nm (the emission maximum of excited pyrene dimer). Concentration of shadows C = 0.128 mg protein/ml. Concentration of pyrene in the suspension is $7.7 \cdot 10^{-6}$ M, temperature of the specimens 309.1±0.1 K (36 °C), pH of the suspension 7.35

To measure the microviscosity of a lipid bilayer near proteins (the region of protein-lipid interaction), we used the excitation wavelength $\lambda = 281$ nm and spectral slit width 1.5/5. Microviscosity of a lipid bilayer far from proteins (the region of lipid-lipid interaction) was measured with the excitation wavelength $\lambda = 337$ nm and spectral slit width 1.5/3. At that, the maxima of emission intensity were observed at $\lambda = 374$ nm and $\lambda = 393$ nm (the vibronic emission peaks of excited pyrene monomers), and $\lambda = 468$ nm (the emission maximum of excited pyrene dimer). Fig. 6 shows the emission spectrum of pyrene in the shadows suspension.

The relative microviscosity of membranes was determined as a ratio $\eta(A)/\eta(0)$, where $\eta(A)$ and $\eta(0)$ are microviscosities of membranes, respectively, with and without hormone added to the shadow suspension. For the region of lipid-lipid interaction, relative microviscosity was calculated by the formula

$$\eta(A)/\eta(0) = \{F_{468}(0)/F_{468}(A)\} \cdot \{F_{393}(A)/F_{393}(0)\} \tag{17}$$

where $F_{468}(A)$ is the fluorescence intensity of pyrene at wavelength $\lambda = 468$ nm in a specimen at the hormone concentration A in suspension; $F_{468}(0)$ is the fluorescence intensity of pyrene at wavelength $\lambda = 468$ nm in a specimen with no hormone in suspension. $F_{393}(A)$ and $F_{393}(0)$ are the fluorescence intensities of pyrene at wavelength $\lambda = 393$ nm at the hormone concentration A in suspension and without hormone in suspension, respectively. The excitation wavelength is 337 nm.

For the region of protein-lipid interaction, relative microviscosity was calculated by the formula

$$\eta(A)/\eta(0) = \{(F_{468}(0) - I_{468})/(F_{468}(A) - I_{468})\} \cdot \{(F_{393}(A) - I_{393})/(F_{393}(0) - I_{393})\} \tag{18}$$

where I_{393} and I_{468} are the fluorescence intensities of tryptophan at wavelength $\lambda = 393$ nm and $\lambda = 468$ nm, respectively. The excitation wavelength is $\lambda = 281$ nm. A relative measurement error for relative microviscosity was equal to 6%.

3.2 Results
3.2.1 IR spectroscopy
The analysis of IR spectra of rat erythrocyte shadows upon cortisol addition showed a ca. 20% increase in the intensity of absorption bands of CO (1655.2 cm^{-1}) and NH bonds (1548 and 3290 cm^{-1}), the effect becoming more pronounced with increasing concentration of the hormone (table 7, figs. 7, 8). The increased intensity of the band at 1655.2 cm^{-1} points to a growing orderliness in membrane proteins caused by the structural transition tangle $\rightarrow$ α-helix. Appearance of absorption band at 1630 cm^{-1} corresponds to β-structure (tangle $\rightarrow$ β-structure transition) at the cortisol concentration 10^{-7} M (fig. 9). The interaction of hormone ligand with protein enhances intermolecular interaction between membrane proteins and phospholipids, and facilitates the formation of lipid-protein clusters.

A shift of stretching vibrations of the peptide bond (NH bond), 3308 $\rightarrow$ 3280 cm^{-1} ($\Delta v = 28$ cm^{-1}), and an increase in its intensity were found, which are caused by the formation of hydrogen bond between cortisol and NH bond of proteins. It forms most likely between the keto group in hormone A-ring (C$_3$ = 0) and NH bond of the membrane protein. Although both the keto group at C$_{20}$ in D-ring and the OH group at C$_{11}$ in C-ring may also participate

in the formation of hydrogen bonds. Cortisol is a cholesterol derivative; however, the presence of two keto and three hydroxy groups considerably changes its interaction with the surface of erythrocyte membrane as compared to cholesterol. The latter penetrates deep into the membrane and enhances the hydrophobic interactions between chains of fatty acids in phospholipids. Cortisol acts on the surface. Of interest are the shifts of CH bond stretching vibrations: $2848 \rightarrow 2852$ cm^{-1} ($\Delta v = 4$ cm^{-1}) and $2930 \rightarrow 2925$ cm^{-1} ($\Delta v = 5$ cm^{-1}). The latter increased also its intensity under the action of hormone. A change in the intensity of this bond confirms the occurrence of structural transition order $\rightarrow$ order under the action of cortisol, but does not reveal where it takes place: in membrane proteins or in phospholipids, since CH bond resides both in proteins and phospholipids. An increase in the intensity of absorption band of C=O bond in phospholipids and its shifting from 1748 to 1740 cm^{-1} were observed. This increase in the band intensity points to an enhanced orderliness of higher carboxylic acids and a decreased entropy in phospholipids. The band shift is caused by the formation of hydrogen bond between the hormone, probably OH group at C_{21}, and CO bond in phospholipids. Such a concurrent interaction of the hormone with protein and phospholipids takes place at the interface of proteins and phospholipids, which enhances the lipid-protein interactions and leads to the formation of complex domains revealed by atomic force microscopy.

A 3 cm^{-1} shift in the frequency of P=O bond to the short-wave region and a minor increase in its intensity were observed.

This is attributed to dehydratation of membranes upon their deformation (compression) under the action of hormone. This is exactly the loss of bound water that increases the frequency of P=O bond. Displacement of water dipoles from lipid-protein domains to adjacent regions results in the appearance of meso-stripes with tensile hydrodynamic stress (see fig. 20).

It is known that spectrin accounts for 30% of membrane proteins (Leto & Marchesi, 1984). It can be expected that additional deformation of membranes would occur due to the spectrin-actin-ankyrin meshwork capable of contraction, this meshwork residing on both the internal and external surfaces of the membrane (Palek & Sahr, 1992). This mechanism of erythrocyte membrane deformation plays a more essential role upon interaction with adrenaline and noradrenaline. Thus, adrenoreceptor and cholinoreceptor were found earlier on the surface of erythrocyte membranes (Leto & Marchesi, 1984). The EPR spectroscopy study revealed that deformation (contraction) of erythrocyte membranes occurs in erythrocyte membranes (shadows) under the action of adrenaline or carbachol (the analog of choline). The contraction effect was eliminated by cytochalasin, which can stabilize spectrin. Later, the IR spectroscopy study showed that carbachol and adrenaline produce changes in the secondary structure of these proteins. In the present study we also observed a similar effect on erythrocyte membranes caused by the action of adrenaline and noradrenaline.

Upon incubation of adrenaline with concentration 10^{-9} M and shadows, we observed shifting of absorption bands of CO and NH groups of the peptide bonds. The CO band shifted from 1655.4 to 1654 cm^{-1}, whereas at $C_{adrenaline} = 10^{-7}$ M the shift was $1655.4 \rightarrow 1656$ cm^{-1}, accompanied by appearance of the band at 1646 cm^{-1}. In the first case, absorption band of NH bond shifted by 32 cm^{-1}, and in the second case, by 36 cm^{-1}. Splitting of the band of NH bonds was also recorded (table 7, figs. 10, 11).
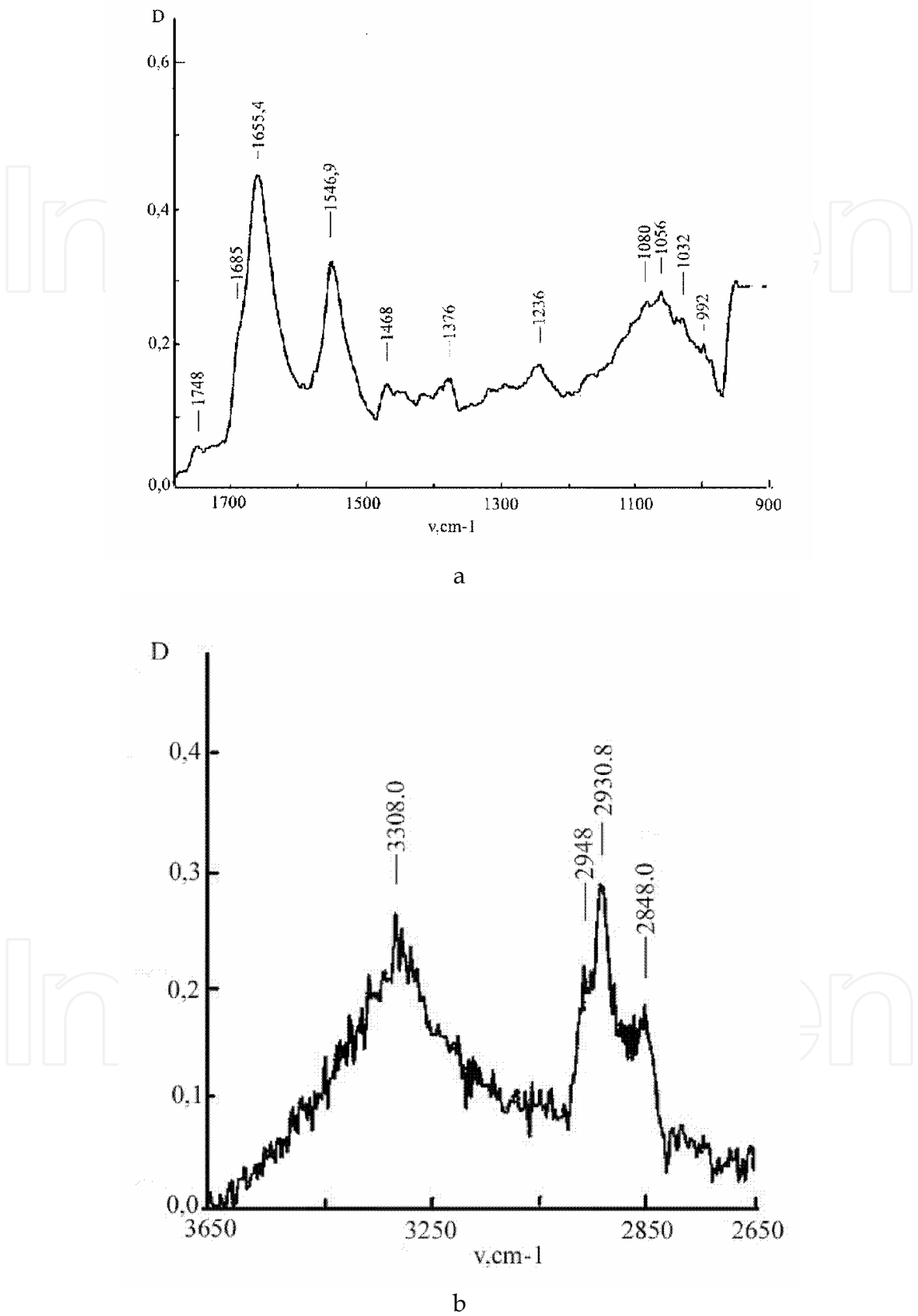
a

b

Fig. 7. IR spectra of rat erythrocyte membranes (control) ($C_{\text{phosph. buff.}}$ = 0.01 M, pH 7.35, relative humidity 0%): a) ν = 900-1800 cm^{-1}, b) ν = 2600-3700 cm^{-1}

Thermodynamics and Mesomechanics of Nanostructural Transitions
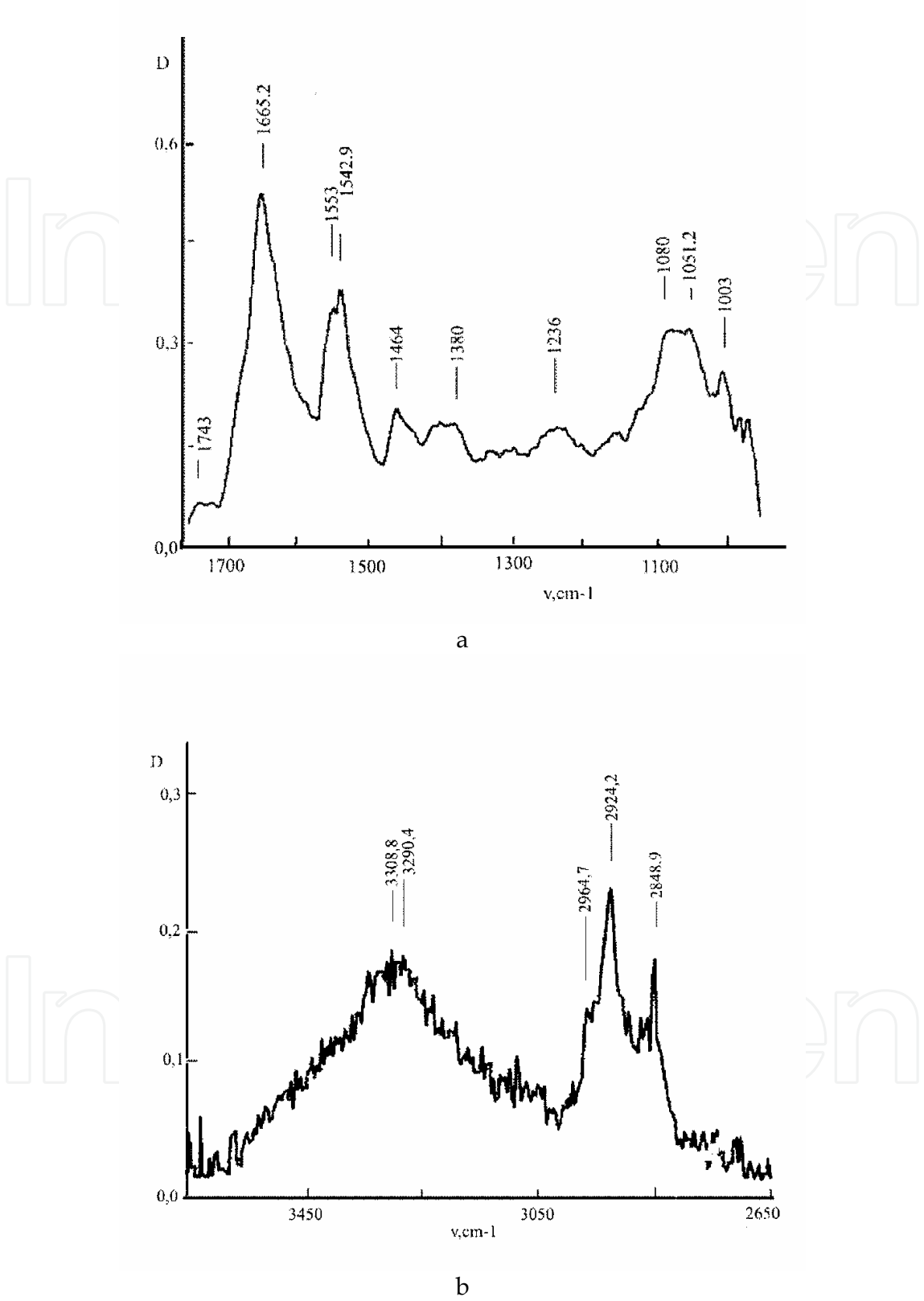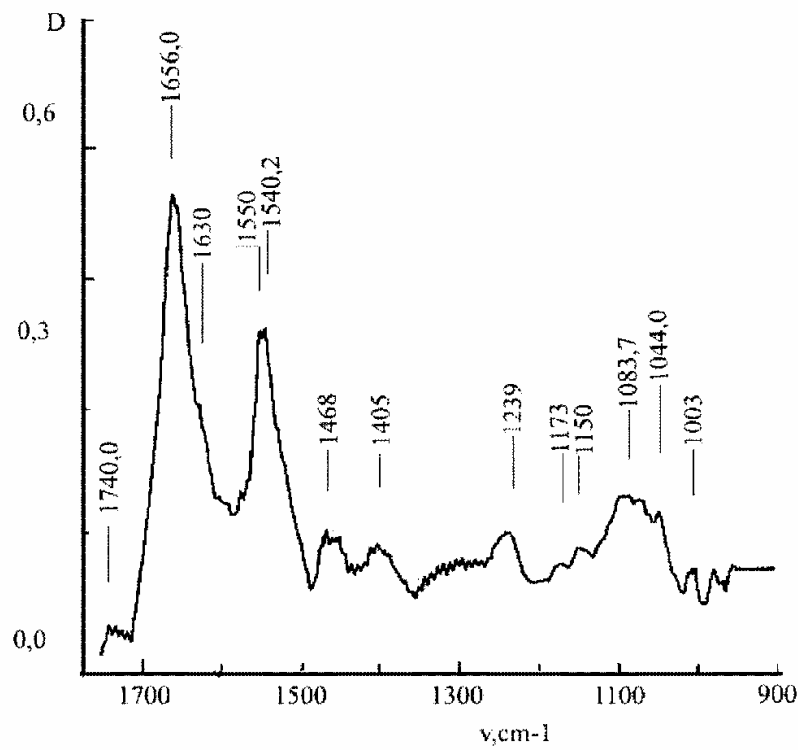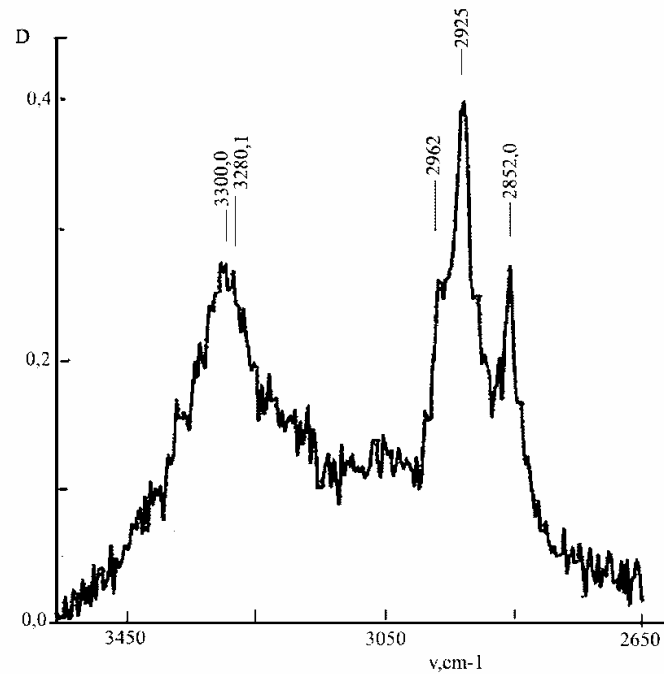in Biological Membranes as Liquid Cristals
331

a

b

Fig. 8. IR spectra of rat erythrocyte membranes incubated with cortisol (C_C = 4.44 x 10^{-8} M, $C_{phosph. buff.}$ = 0.001 M, pH 7.35, relative humidity 0%): a) ν = 900-1800 cm^{-1}, b) ν = 2600-3700 cm^{-1}
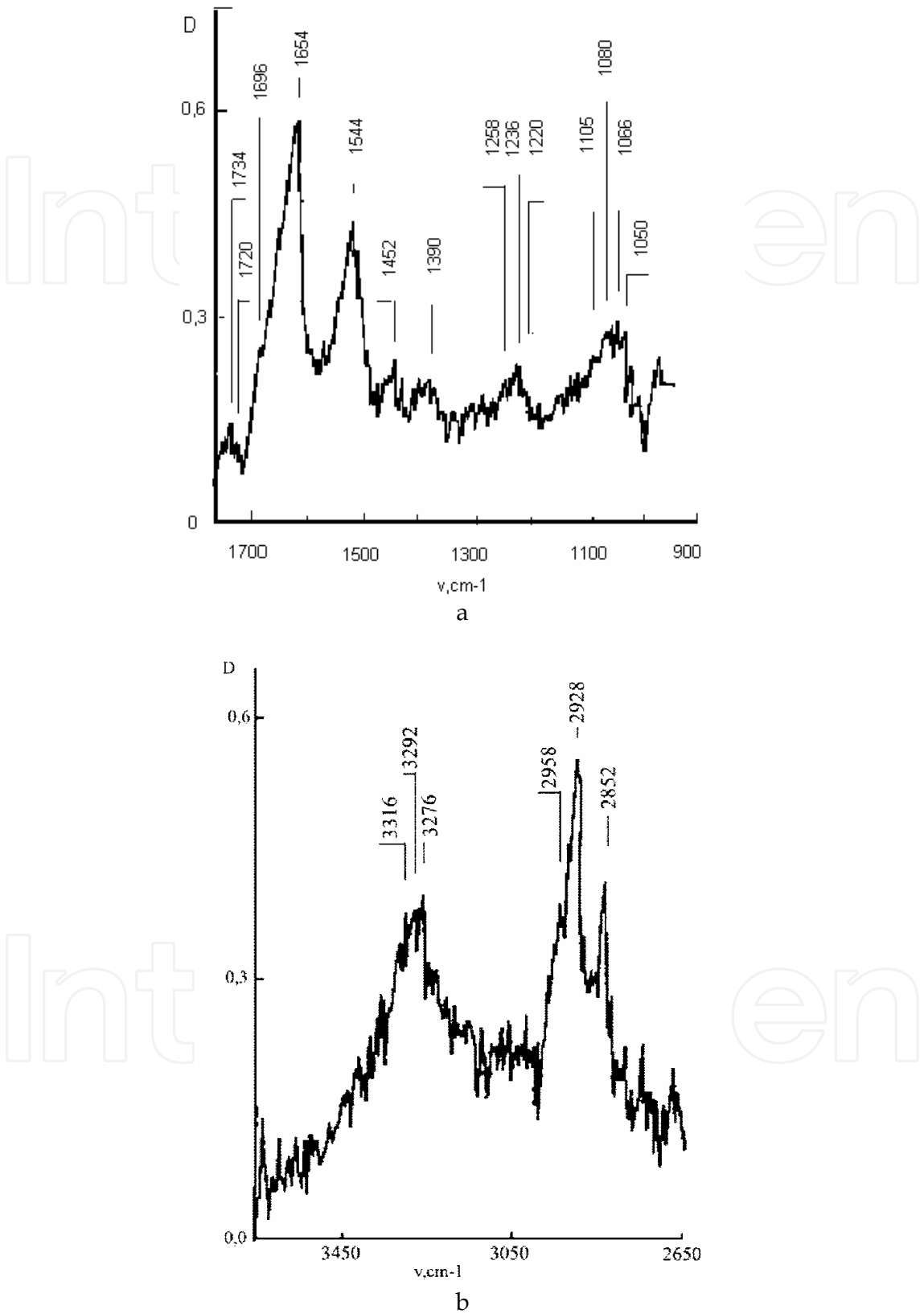
Fig. 9. IR spectra of rat erythrocyte membranes incubated with cortisol (C_C = 1.05 x 10^{-7} M, $C_{phosph.\ buff.}$ = 0.001 M, pH 7.35, relative humidity 0%): a) v = 900-1800 cm^{-1},
b) v = 2600-3700 cm^{-1}

Interestingly, the low concentration of adrenaline gave a 28 cm^{-1} shift of the band of phospholipid CO bonds, whereas with noradrenaline this value was only 18 cm^{-1}. Splitting of the band was also observed. At the same time, the absorption band of PO bond showed strong splitting (table 7, fig. 10). Its shift to the short-wave region was 22 cm^{-1}, and to the long-wave region, 16 cm^{-1}. Upon splitting, the band shift between extreme bands attained 38 cm^{-1}.

Absorption band in the region of 2928 cm^{-1} (CH stretching vibrations) showed an additional splitting. Bands shifting was also recorded in this part of the spectrum.

Incubation of noradrenaline with erythrocyte shadows was accompanied by shifting of absorption bands assigned to the peptide bond of membrane proteins, in particular, the 1655.4 → 1654 cm^{-1} shift of CO bond ($\Delta v = 1.4$ cm^{-1}) and 3308 → 3270 cm^{-1} shift of NH bond (stretching vibrations) ($\Delta v = 38$ cm^{-1}) (table 7, fig. 12). Shifting of the indicated absorption bands points to conformational transitions in membrane proteins: tangle → α-helix and tangle → β-structure. The bands at 1654 and 1685 cm^{-1} increased in intensity as well as the band of NH bond (amide II) at 1548 cm^{-1}. In addition, splitting in the region of NH bond (stretching vibrations) was observed. This splitting indicates the mutual interaction of intramolecular domains comprising α-helices or β-structures, which results from their ordering. However, the splitting may be related also with intermolecular interaction of proteins. Deformation or contraction of membrane under the action of noradrenaline takes place here, similar to the case of adrenaline, thus leading to pronounced changes in the structure of membrane proteins. These changes may be caused by interaction of several functional groups of noradrenaline with the receptor, in particular, amino group and OH groups. Hydrophobic interaction of the aromatic ring of noradrenaline with hydrophobic region of its receptor is also possible.

The 1748→1730 cm^{-1} band shift of phospholipid C=O bond was recorded as well as the 1236→1246 cm^{-1} shift of phospholipid P=O bond. The band of P-O-C bond also shifts by 16 cm^{-1} to the short-wave region of the spectrum. So strong shifting of these bands results from the increased ordering of phospholipids. However, this is caused also by the enhanced interaction with membrane proteins, in particular, integral proteins, protein of stripe 3, and finally with retraction proteins. Note that hydrogen bonds are formed with any of these proteins. Probably the receptor for adrenaline may have not only the protein, but also the protein-lipid nature. If this is the case, OH groups of noradrenaline will interact with C=O or P=O bonds.

Shifting of absorption band of $O_4C_4C_5O_5$ in monosaccharides was recorded (1056 → 1072 cm^{-1}, $\Delta v = 16$ cm^{-1}). This shift indicates the formation of hydrogen bonds of noradrenaline with the functional groups of monosaccharides as well as the ordering of monosaccharides relative to each other accompanied by changes in their conformation, such as boat → chair. The chair conformation is energetically more advantageous.

Note. A_{CO} is the integral intensity of v_{CO} absorption band of peptide bond on semi-log scale. Thus, the comparison of adrenaline and noradrenaline effect shows that action of the first hormone on phospholipids is more pronounced as compared to the second hormone. This is related with the presence of methyl radical at nitrogen due to higher electronegativity of nitrogen atom, charge of the methyl group increases, thus enhancing the effect of adrenaline on the membrane. This gives ground to suggest that amino group and methylamino group interact with phospholipids by CO and PO bonds.

The total effect of all the hormones is presented in table 7.

Compound	ν_{CO} (cm^{-1})	ν_{NH} stretch. (cm^{-1})	$\nu_{C=O}$ (cm^{-1})	$\nu_{P=O}$ (cm^{-1})	$\nu_{P\text{-}O\text{-}C}$ (cm^{-1})	NO_4C_4-C_5O_5 (cm^{-1})	ν_{CH} stretch. (cm^{-1})	A_{CO}
Shadows (control)	1655.4 1686	3308	1748	1236	1080	1056	2948 2930 2848	*1.2150E + 01*
Shadows + cortisol (A = 4.4 ·10^{-8} M)	1655.2	3290.4 3308.0	1743	1236	1080	1051.2	2924.2 2848.9	*1.5169E + 01*
Shadows + cortisol (A = 1.05 ·10^{-7} M)	1656.0 1630	3280 3300	1740	1239	1083.7	–	2962 2925 2852	*1.5640E + 01*
Shadows + cortisol (A = 2 ·10^{-7} M)		3280 3296					2952.5 2931.4 2920.0 2853.8	
Shadows + adrenaline (A = 10^{-9} M)	1654	3276 3292 3316	1720 1734 1744	1220 1236 1244 1258	1080 1088 1094	1066	2958 2952 2928* 2852	
Shadows + adrenaline (A = 10^{-7} M)	1656 1646	3272 3288 3304 3320	1740	1220 1236 1248 1258	1080 1096	1070 1060 1044	2956 2924 2852	
Shadows + noradrenaline (A = 1.87 ·10^{-7} M)	*1654*	*3271 3300*	*1730*	*1246*	*1096*	*1072*	*2952 2928 2852*	

Table 7. IR spectroscopy. Frequency parameters of rat erythrocyte shadows after their interaction with hormones

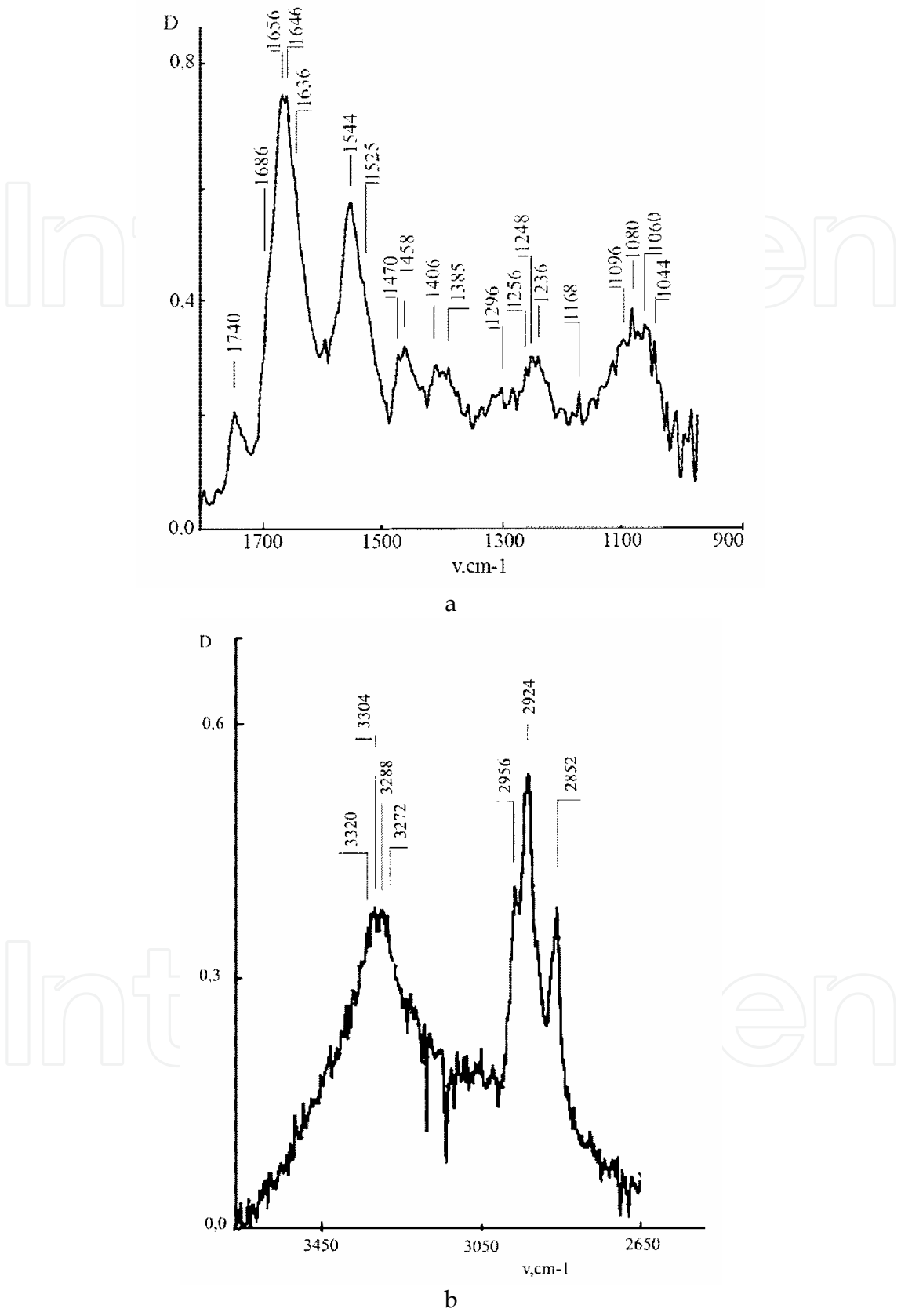Fig. 10. IR spectra of rat erythrocyte membranes incubated with adrenaline ($C_A = 10^{-9}$ M, $C_{phosph.\ buff.} = 0.001$ M, pH 7.35, relative humidity 0%): a) $\nu = 900\text{-}1800$ cm^{-1}, b) $\nu = 2600\text{-}3700$ cm^{-1}
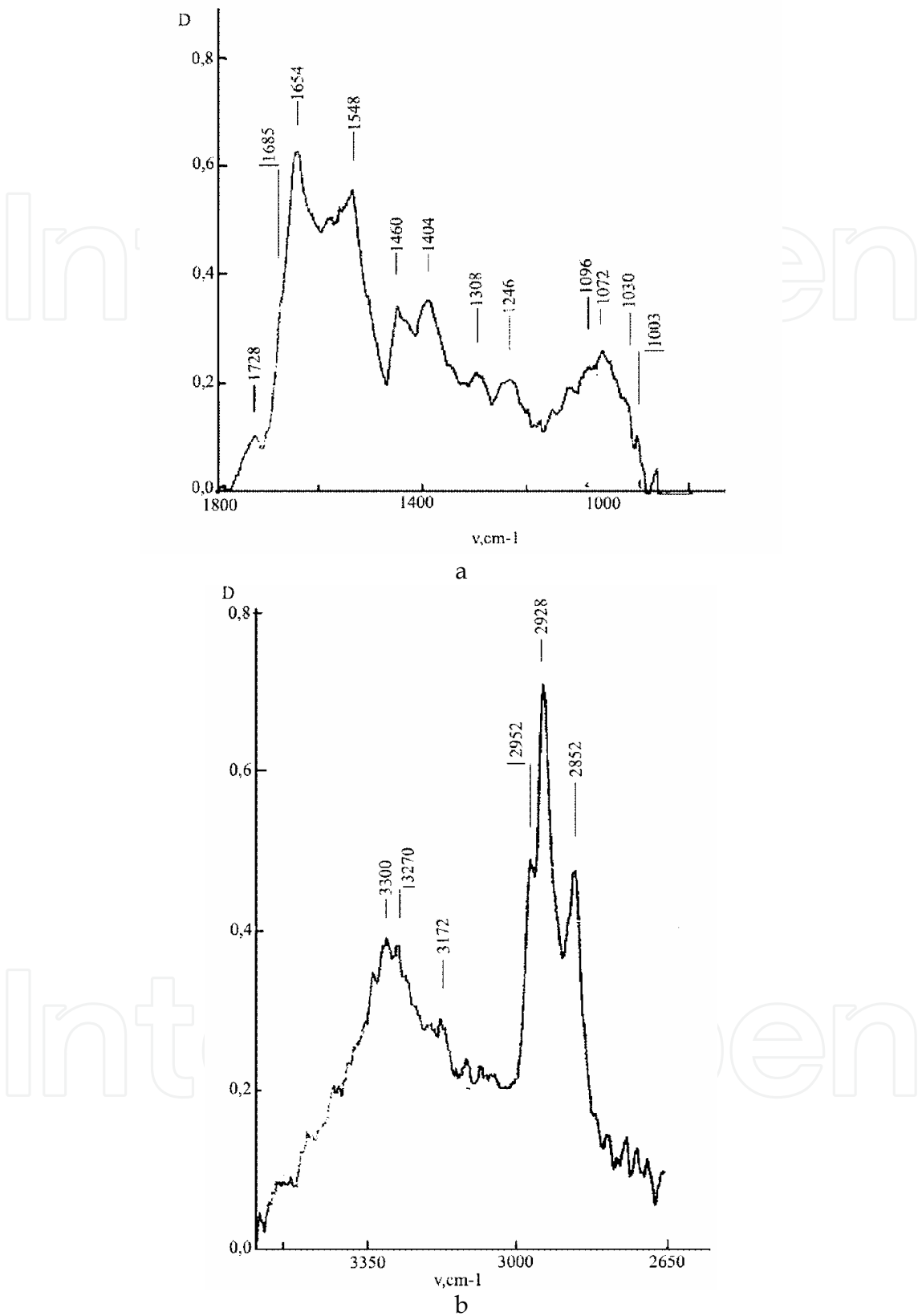
Fig. 11. IR spectra of rat erythrocyte membranes incubated with adrenaline ($C_A = 10^{-7}$ M, $C_{phosph.\ buff.} = 0.001$ M, pH 7.35, relative humidity 0%): a) $\nu = 900\text{-}1800$ cm^{-1}, b) $\nu = 2600\text{-}3700$ cm^{-1}

Fig. 12. IR spectra of rat erythrocyte membranes incubated with noradrenaline (C_{NA} = 1.87 x 10^{-7} M, $C_{phosph. buff.}$ = 0.001 M, pH 7.35, relative humidity 0%): a) ν = 900-1800 cm^{-1}, b) ν = 2600-3700 cm^{-1}

Fluorescence analysis allowed us to observe the contribution of proteins to initiation of structural transitions in erythrocyte membranes under the action of hormones. For this purpose we used both the effect of light absorption and the tryptophan fluorescence quenching when determining the protein secondary structure.

3.2.2 Fluorescence analysis

As was noted above, cortisol cannot penetrate deep into phospholipid bilayer and interacts with proteins on the surface of cell membrane. This leads to pronounced transformation of their secondary structure and is accompanied by a decrease in the absorption maximum at 228 nm. Addition of hormone to the incubation medium with the concentration $1.82 \cdot 10^{-7}$ M decreased the absorption intensity by 30 a.u., which made up 4.6% as compared to control (the hypochromic effect). The hypochromic effect is related with transition of protein molecule from static tangle to α-helix (Panin & Panin, 2007), i.e., with increased orderliness of its structure.

The absorption spectrum of macromolecules, which have an ordered structure in the excited state, reflects the interaction between excited monomeric units and strongly depends on their spatial arrangement in the molecule.

The structural transitions in proteins at cortisol interaction with erythrocyte membranes are evidenced also by the curves of tryptophan fluorescence quenching. A maximum of fluorescence decrease was observed at the hormone concentration in the incubation medium equal to $11.6 \cdot 10^{-8}$ M and the protein content of 0.256 mg/ml, ΔF was 34 a.u., which makes up 11% with respect to control (fig. 13).
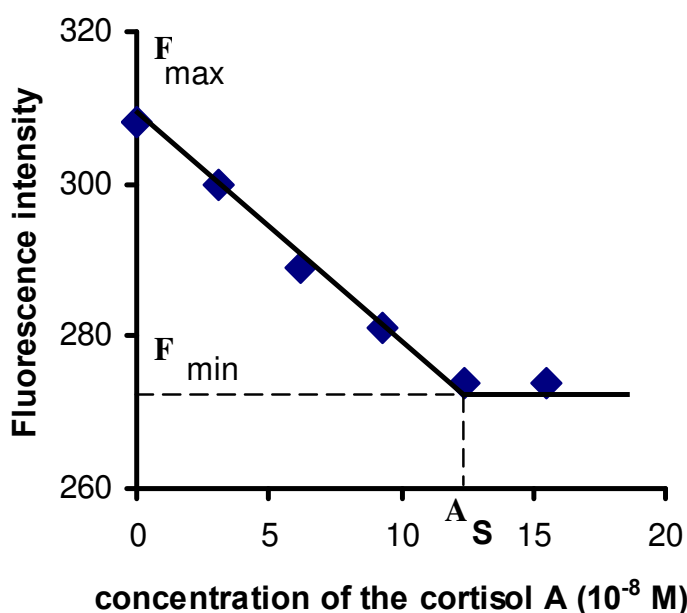

Fig. 13. The dependence of fluorescence intensity of shadows on the concentration *A* of hormone cortisol introduced into the cuvette. A_s is the stoichiometric concentration of the hormone. Concentration of membrane protein C = 0.256 mg/ml. The excitation wavelength λ = 281 nm, emission wavelength λ = 332 nm

The data on tryptophan fluorescence quenching were used to calculate the constants of hormone binding (K_b), the amount of bound hormone (B_{max}, mol/mg of protein), and a change in free energy (ΔG, kJ/mol) upon interaction of cortisol with erythrocyte membrane

(table 8). It was found that K_b for cortisol is $(1.23 \pm 0.12) \cdot 10^6$ M^{-1}. A similar value for transcortin (a specific receptor) is $3 \cdot 10^7$ M^{-1} (Panin & Panin, 2004), which is an order of magnitude higher. However, even in the norm, 6-8% of the hormone is bound to blood cells. These are mainly erythrocytes. Under stress, this value may rise considerably. Our calculations showed that the maximal saturation of erythrocyte membranes with hormone (B_{max}) in vitro is $(4.7 \pm 0.47) \cdot 10^{-10}$ mol/mg of protein, which is quite a low value (table 8). When cortisol interacts with erythrocyte membranes, free energy of the entire system (ΔG) decreases by 30.0 kJ/mol. This indicates that under the action of hormone the orderliness of structural components in erythrocyte membranes increases, whereas their entropy decreases.

Hormone	Binding constant K_b (M^{-1})	Amount of bound hormone B_{MAX} (mol/mg protein)	Changes in Gibbs free energy ΔG (kJ/mol)
Cortisol	$(1.23 \pm 0.12) \cdot 10^6$	$(4.69 \pm 0.47) \cdot 10^{-10}$	– 36.0
Adrenaline	$(6.3 \pm 0.63) \cdot 10^6$	$(1.60 \pm 0.16) \cdot 10^{-11}$	– 40.2
Noradrenaline	$(1.70 \pm 0.17) \cdot 10^6$	$(8.10 \pm 0.81) \cdot 10^{-10}$	– 36.9

Table 8. Parameters of cortisol binding to erythrocyte membrane based on tryptophan fluorescence quenching of membrane proteins and parameters of adrenaline and noradrenaline binding to erythrocyte membrane based on the hypochromic effect of tryptophan in membrane proteins
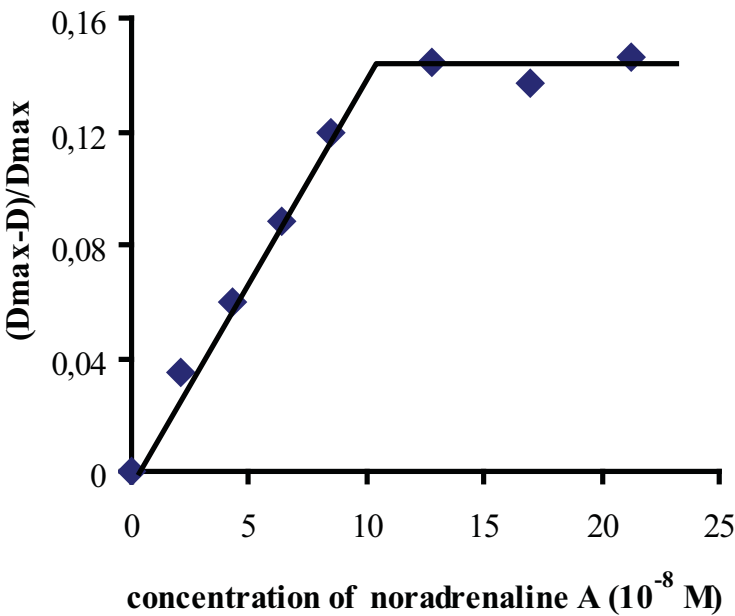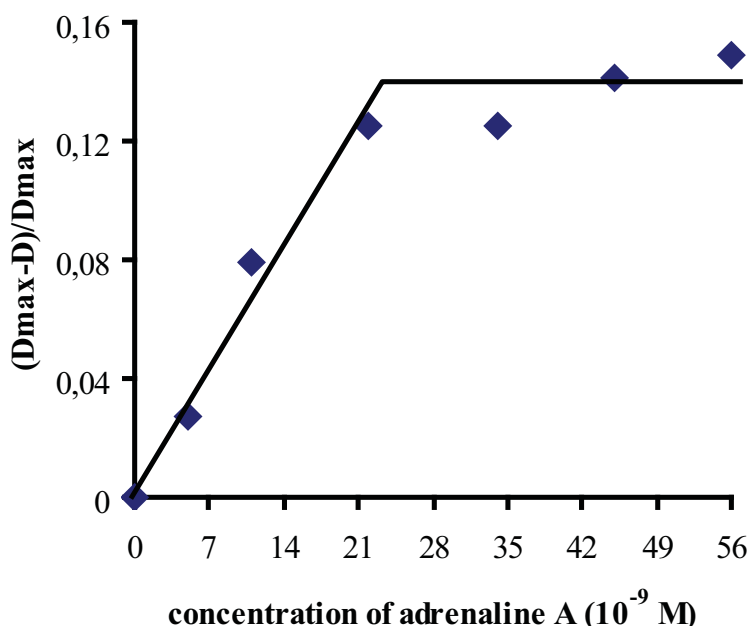

Fig. 14. The dependence of $(D_{max}-D)/D_{max}$ on the concentration A of hormone noradrenaline introduced into the cuvette. Here, D_{max}, D - are the intensities of tryptophan absorption in shadows at λ = 228 nm, respectively, without addition of hormone and with hormone. Concentration of membrane protein C = 0.124 mg/ml. The emission wavelength λ = 332 nm

Similar results were obtained in our study of two other stress hormones, adrenaline and noradrenaline. With both hormones, the hypochromic effect is even more pronounced than with cortisol (table 8, figs. 14, 15). This suggests an increased orderliness of the membrane proteins structure due to transition tangle $\rightarrow$ β-structure $\rightarrow$ α-helix. A decrease in absorption may be related with changes in the dipole moments direction of quantum transitions of monomeric protein residues accompanying their transition into another conformation.

Fig. 15. The dependence of $(D_{max}\text{-}D)/D_{max}$ on the concentration A of hormone adrenaline introduced into the cuvette. Here, D_{max}, D - are the intensities of tryptophan absorption in shadows at λ = 228 nm, respectively, without addition of hormone and with hormone. Concentration of membrane protein C = 0.124 mg/ml. The emission wavelength λ = 332 nm

Due to high intrinsic fluorescence of the hormones, their effect on tryptophan fluorescence quenching cannot be revealed. Nevertheless, the absorption measurements allowed us to calculate K_b, B_{max} and ΔG for these hormones. Overall, they were of the same order of magnitude as those for cortisol. Adrenaline showed a higher value of K_b, a lower amount of bound hormone (B_{max}), and more pronounced changes of ΔG (– 40.2 kJ/mol). The latter fact testifies that adrenaline increases the orderliness of structural components in erythrocyte membranes to a greater extent than other hormones. It provided also a stronger deformation of erythrocyte membranes, which agrees with the data of atomic force microscopy (see figs. 24, 25). It was vital to relate structural transitions in erythrocyte membranes under the action of stress hormones with changes in their elasticity and viscosity.

3.2.3 Changes in microviscosity of erythrocyte membranes under the action of cortisol and catecholamines

The addition of cortisol, adrenaline or noradrenaline to erythrocyte shadows increased microviscosity of erythrocyte membranes (figs. 16, 17). The effect was more pronounced in the presence of adrenaline (an increase by 40%) and less pronounced in the presence of noradrenaline (by 24%) and cortisol (by 25%). Adrenaline was able to increase the membrane microviscosity at a much lower concentration of hormone in the incubation

medium. With adrenaline, a plateau was reached at the hormone concentration of $1.7 \cdot 10^{-9}$ M, whereas with noradrenaline and cortisol at $7 \cdot 10^{-8}$ M.
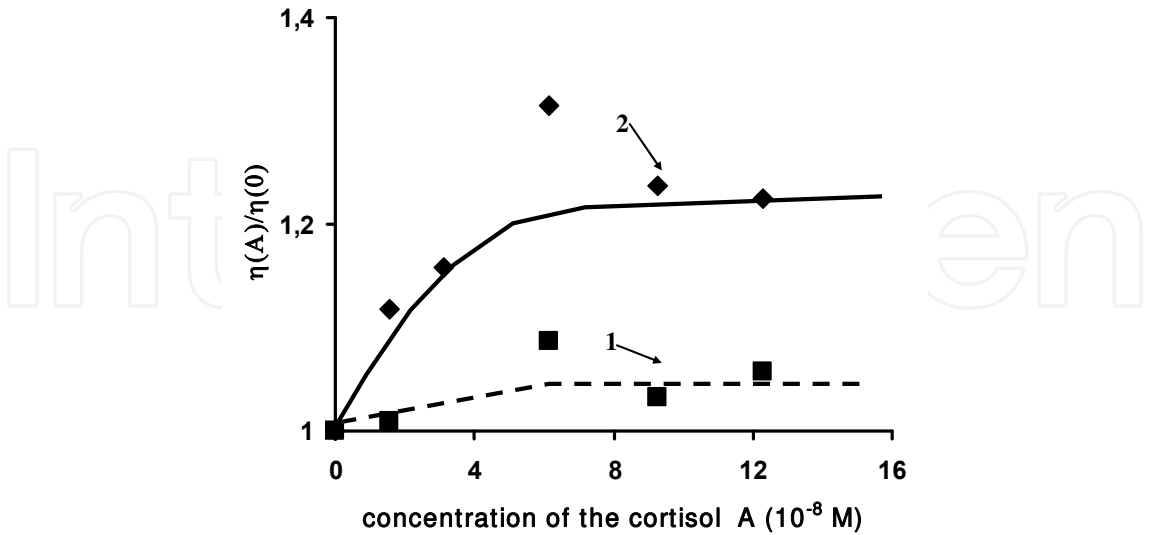

Fig. 16. Changes in the relative microviscosity of membranes $\eta(A)/\eta(0)$ of erythrocyte shadows at the concentration A of hormone cortisol, where $\eta(A)$ and $\eta(0$ are microviscosities of the membranes, respectively, with cortisol added to the shadows suspension and without hormone. Concentration of shadows C = 0.128 mg protein/ml. Line 1 – changes of relative microviscosity in the region of lipid-lipid interaction, line 2 – changes of relative microviscosity in the region of protein-lipid interaction. Concentration of pyrene in the suspension is $7.7 \cdot 10^{-6}$ M, temperature of the specimens 309.1±0.1 K (36 °C), pH of the suspension 7.35. The measured value of $\eta(A)/\eta(0)$ exhibits error of 6%
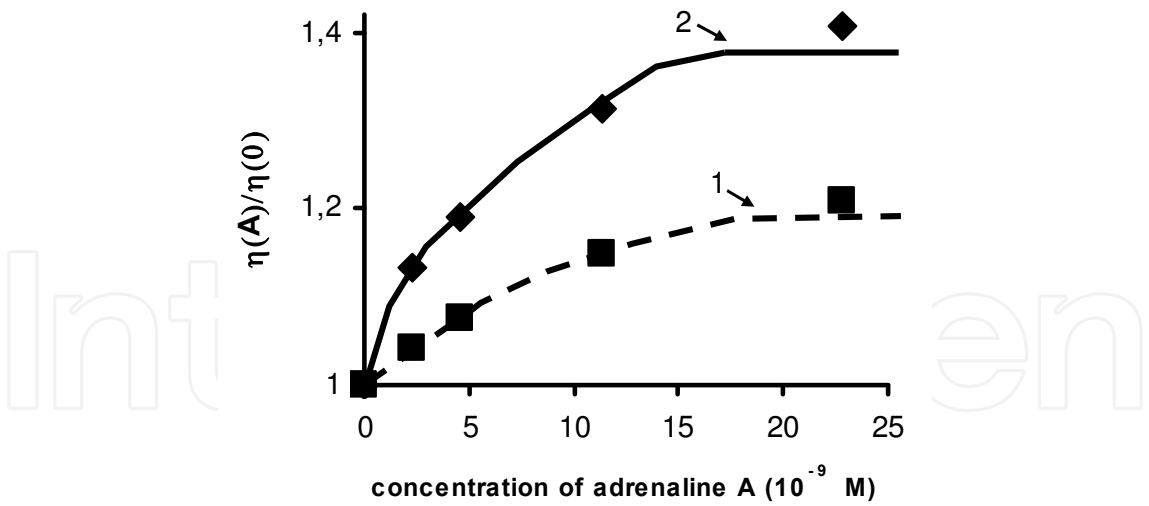

Fig. 17. Changes in the relative microviscosity of membranes $\eta(A)/\eta(0))$ of erythrocyte shadows at the concentration A of hormone adrenaline, where $\eta(A)$ and $\eta(0)$ - are microviscosities of the membranes, respectively, with adrenaline added to the shadows suspension and without hormone. Concentration of shadows C = 0.128 mg protein/ml. Line 1 – changes of relative microviscosity in the region of lipid-lipid interaction, line 2 – changes of relative microviscosity in the region of protein-lipid interaction. Concentration of pyrene in the suspension is $7.7 \cdot 10^{-6}$ M, temperature of the specimens 309.1±0.1 K (36 °C), pH of the suspension 7.35. The measured value of $\eta(A)/\eta(0)$ exhibits an error of 6%

For all the hormones, in the region of lipid-protein interactions microviscosity increased at lower concentrations and was more pronounced than in the region of lipid-lipid interactions (fig. 16, 17). An increase in microviscosity of erythrocyte membranes correlated with a decrease of tryptophan absorption in membrane proteins (fig. 13, 14, 15).

Presumably, structural transitions in erythrocyte membranes under the action of stress hormones are initiated to a greater extent in proteins and to a less extent in lipids.

3.2.4 Atomic force microscopy

Under atomic force microscope, erythrocytes of healthy animals looked as large biconcave discs ca. 6 μm in diameter, which agrees with the results obtained by other authors (Wu et al., 2009). At a higher magnification, their surface showed a slight nonuniformity caused most likely by the presence of membrane proteins. When the erythrocyte suspension was supplemented with DMS and ethanol (0.25% of the mixture volume), the surface nonuniformity increased, probably due to denaturating effect of solvent on the surface structural proteins (figs. 18, 19). The pattern changed drastically upon addition of cortisol to erythrocyte suspension with the final concentration 10^{-6} M. On a smooth surface, there appeared numerous meso-stripes loosening the cell membrane structure (figs. 20, 21). These meso-stripes are ca. 7 nm hollows in erythrocyte membrane. They divide the erythrocyte membrane into flat domains.
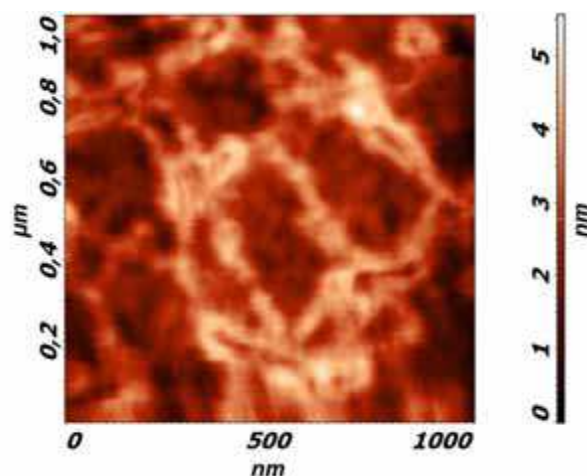

Fig. 18. The control surface of rat erythrocyte. The erythrocyte suspension was supplemented with DMS and ethanol (0.25% of the mixture volume), the surface nonuniformity increased, probably due to denaturating effect of solvent on the surface structural proteins. Scan size 1x1 μm^2

Adrenaline produced more abrupt changes in the structure of erythrocyte membranes (figs. 22, 23). The membrane surface lost its flatness, there appeared convex domains with quasi-staggered arrangement alternating with considerable hollows on the surface. The addition of adrenaline led to domains of size 250 x 250 nm, with smaller domains on the surface of large ones: size 50 x 50 μm^2 and height 5 nm. Noradrenaline caused the formation of domains with the size 100 x 100 μm and height 2 nm (figs. 24, 25).

IR spectroscopy allowed us to reveal the nature of these structural transformations.
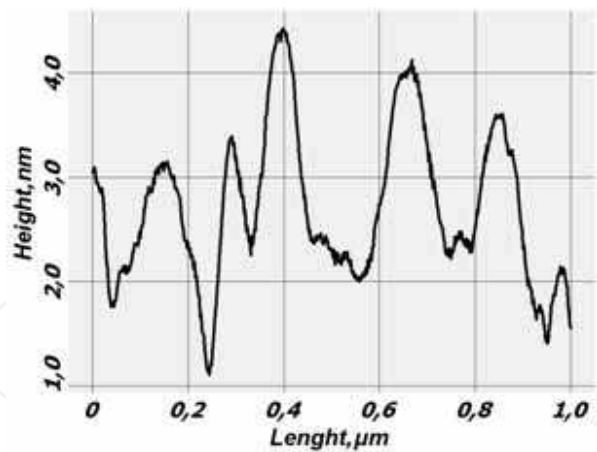
Fig. 19. Center section of the control surface of rat erythrocyte. Section is made from left to right through the center of scan in Fig. 18. Domains with the length 200-250 nm and height 2 nm are seen
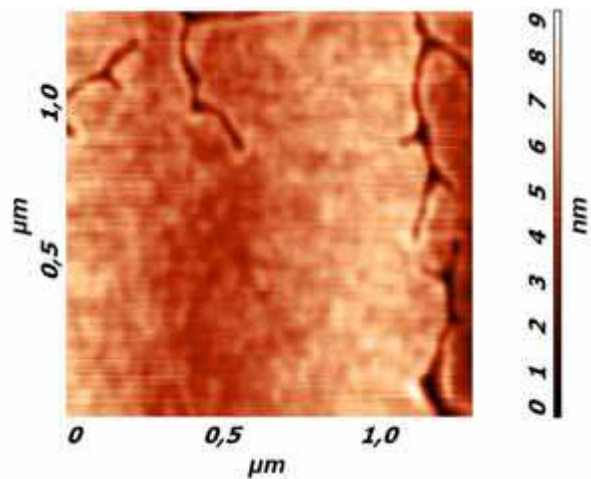

Fig. 20. The surface of rat erythrocyte after adsorption of cortisol. Concentration of the hormone is 10^{-6} M. Scan size 1.3x1.3 μm^2. Deep meso-stripes with bifurcations are seen.
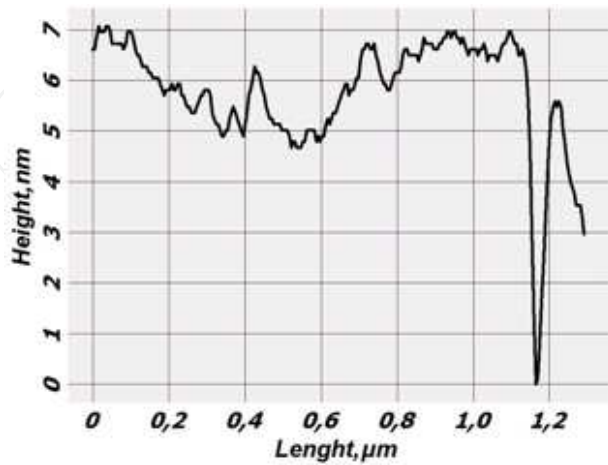

Fig. 21. Center section of the surface of rat erythrocyte after adsorption of cortisol. Section is made from left to right through the center of scan in Fig. 20. The surface is flat, there are hollows of 7 nm depth that divide membrane into domains

3.2.5 Conclusion

Nonspecific mechanisms of the stress hormones interaction with erythrocyte membranes were studied by means of atomic force microscopy, fluorescence analysis, and IR spectroscopy. It was shown that stress hormones (cortisol, adrenaline, noradrenaline) can bind to erythrocyte membranes with high affinity ($K_b \square 10^6$ M^{-1}). The binding mechanism involves hydrogen bonds and hydrophobic and electrostatic interactions.

Active groups of the hormones (NH$_2$, NHCH$_3$, keto, and hydroxy groups) interact simultaneously with CO and NH groups both of proteins and phospholipids. This leads to the formation of complex protein-lipid domains that distort the surface of the erythrocyte membrane. Water dipoles are displaced from the domains to adjacent regions and facilitate membrane loosening. The interaction of hormones with the membrane is accompanied by structural transitions of disorder - order (tangle - α-helix, tangle -β-structure) in membrane proteins and structural transitions of order - order in phospholipids. Formation of large domains (clusters) of the lipid-protein and lipid-lipid nature leads to distortion of membranes and deteriorates their elasticity and rheological properties.
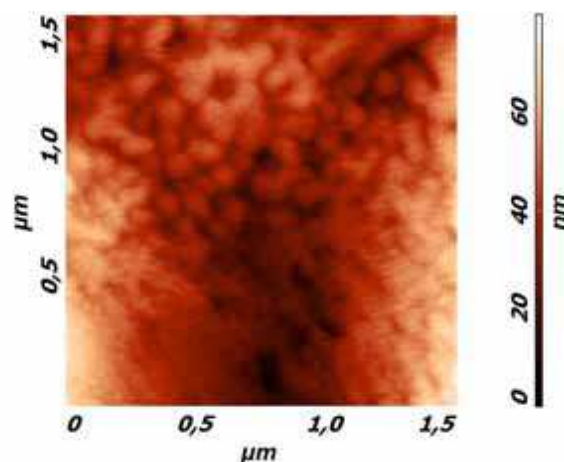

Fig. 22. The surface of rat erythrocyte after adsorption of adrenaline. Concentration of the hormone is 10^{-6} M. Scan size 1.5x1.5 µm^2
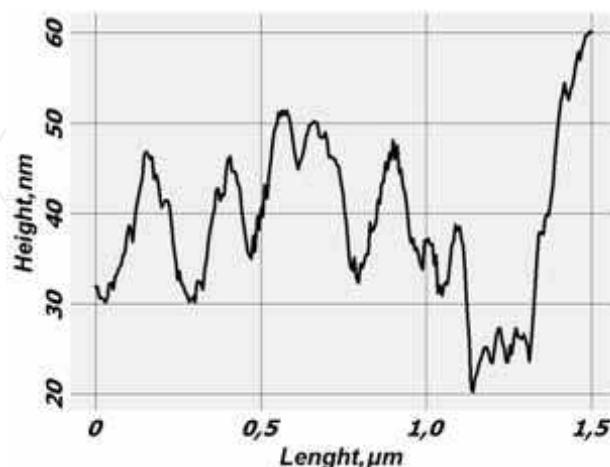

Fig. 23. Center section of the surface of rat erythrocyte after adsorption of adrenaline. Section is made from left to right through the center of scan in Fig. 22. The surface is tuberous, there are domains of size 250 x 250 nm, with smaller domains on the surface of large ones: size 50 x 50 µm^2 and height 5 nm
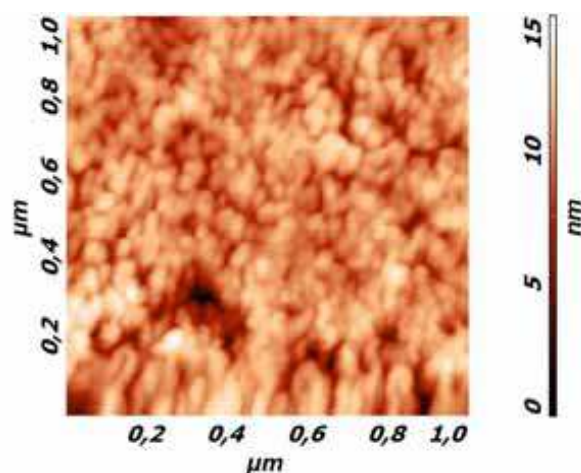
Fig. 24. The surface of rat erythrocyte after adsorption of noradrenaline. Concentration of the hormone is $4 \cdot 10^{-7}$ M. Scan size 1x1 μm²
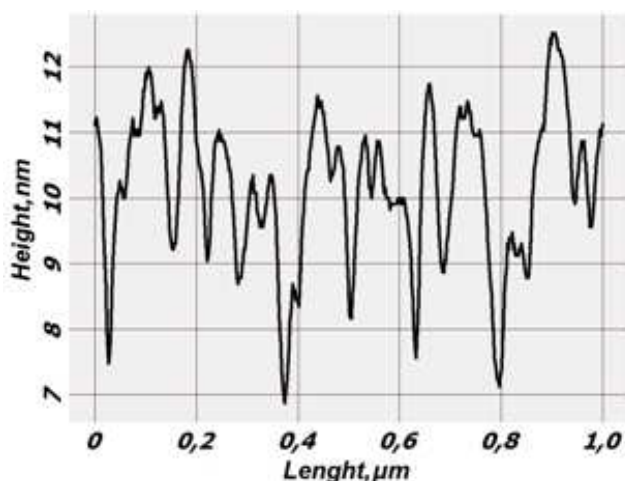

Fig. 25. Center section of the surface of rat erythrocyte after adsorption of noradrenaline. Section is made from left to right through the center of scan in fig. 24. The surface is flat, there are domains of size 100 x 100 μm and height 2 nm

4. Mesomechanics of nanostructural transitions in erythrocyte membranes under the action of metal oxide nanoparticles

The use of nanotechnologies in modern society strongly increased the risk of nanoparticles interaction with the cell membranes of human organism. We studied the effect of metal oxide nanoparticles (SiO_2, ZrO_2) on intact erythrocytes. Such particles possess hydrophobic properties. Nanoparticles of size 5-10 nm penetrate deep into the phospholipid bilayer, which leads to formation of localized deformation meso-stripes (microcracks) (fig. 26b, 26c.). Their formation mechanism also implies the displacement of water dipoles to adjacent regions and membrane loosening due to hydrostatic forces.

Similar fragmentation and fracture is observed in solid crystals in the fields of strong external action. Fig. 26d shows the formation of a domain structure in the bulk of highly nonequilibrium nanostructural aluminium and chains of micropores at its surface layer under severe plastic deformation. Increasing the strain degree causes fracture of the

nanostructural material along the porous bands of the local plastic strain (Panin & Egorushkin, 2008).

As shown by experiments, the addition of Al_2O_3 nanocrystals was not accompanied by reliable changes in microviscosity. However, the addition of SiO_2 nanocrystal initiated on the average a 25% decrease in microviscosity both in the region of lipid-lipid and in the region of protein-lipid interaction. A minor rise of microviscosity at the end of the curve is related with strong damage of the membrane and fluorescence of pyrene that "fell out" to the buffer solution and emits light there. In the buffer, the formation of pyrene dimers is more difficult, so the intensity of fluorescence at a wavelength of 468 nm decreases, whereas relative microviscosity increases. Thus, the rise of microviscosity can be attributed to details of the experimental procedure.
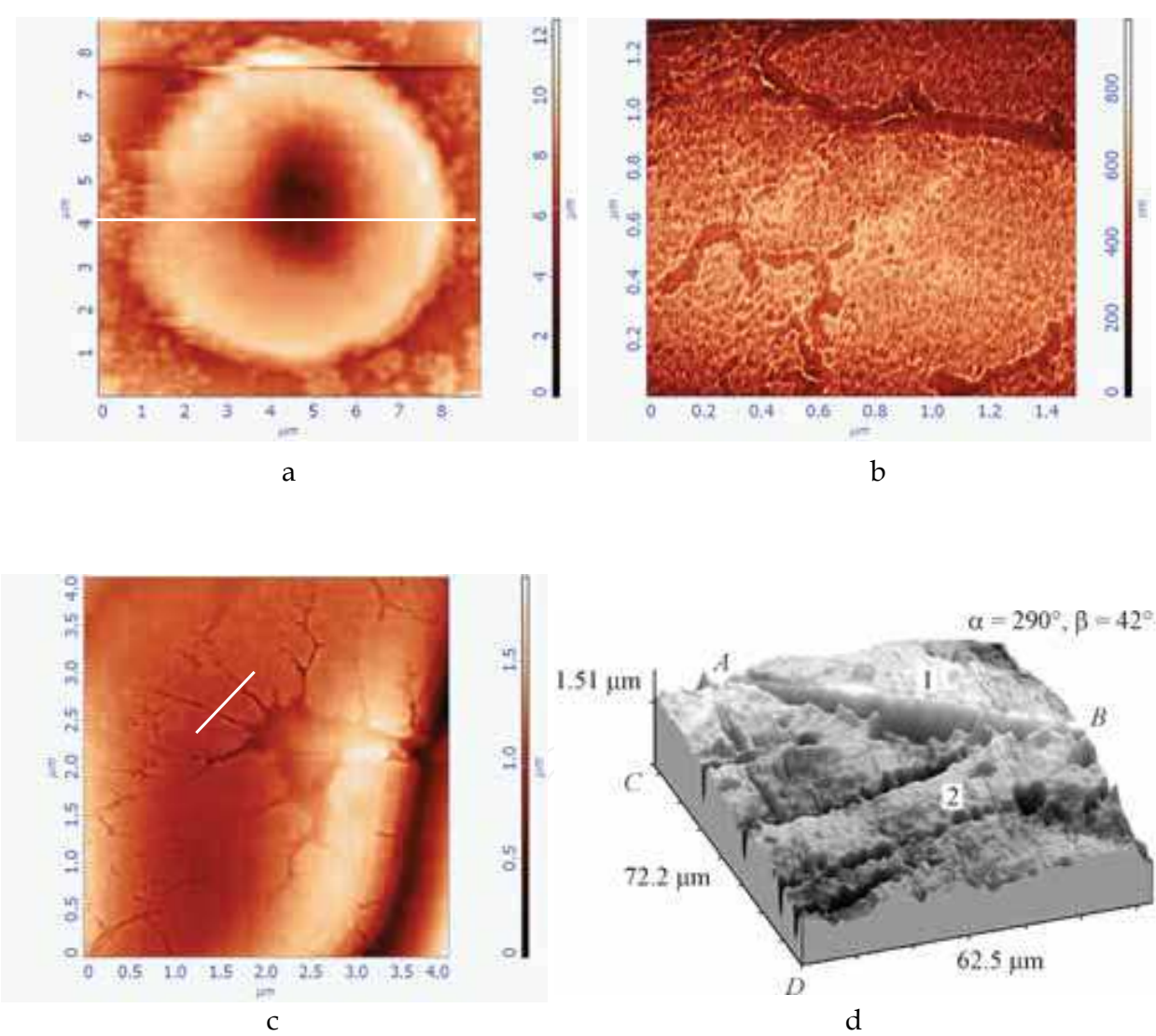

a   b

c   d

Fig. 26. Structural levels of deformation in liquid and solid crystals
a. intact erythrocyte; formation of localized deformation meso-stripes in erythrocyte under the action of SiO_2 (b) and ZrO_2 (c); formation of micropores and their integration into localized deformation meso-stripes in a sample of commercial Al (d), alternating bending, $17.5 \cdot 10^6$ cycles (Panin & Egorushkin, 2008)

5. Thermodynamics of structural transitions in liquid and solid crystals in the fields of external action

Liquid and solid crystals are homeostatic determinate systems (Panin, 2008).

"Classical thermodynamics leads to the notion of system in equilibrium, such as, e.g., crystal" (Nicolis & Prigogin, 1979). In solid crystals residing in the fields of weak external action, the state of homeostasis is determined by the nature of interatomic interactions. This is the metallic bonding, which has a quantum-mechanical nature. It is responsible for the high shear strength of crystals. According to the literature (Panin & Egorushkin, 2008; Shaniavski, 2007), solid crystal in the fields of strong external action behaves as an open thermodynamically nonequilibrium system. "Pumping" of external energy results in a local loss of shear strength, which is accompanied by local structural-phase transformations in the crystal lattice. The possibility of such transformations is determined by electron energy spectrum of the crystal. This is confirmed by a relationship between packing-defect energy (γ) of the crystal and its electronic structure, i.e., memory elements of the crystal (Panin et al., 1971; Panin, 2008). In solid crystals, which are a structurally inhomogeneous medium, structural-phase transitions occur mainly on the external surface and at the internal interfaces. This is the place where a chessboard distribution of stresses and deformations is formed: the cells under compressive normal stress alternate chequerwise with the cells under tensile normal stress (Panin & Panin, 2007). Tangential stresses also have a chessboard distribution, which is spatially displaced in phase by $\pi/2$. This can explain the physical nature of plastic flow localization at different scale-structural levels under different conditions of loading. The excess molar volume and virtual nodes of a higher energy structure in the interstitial space that are present in the zones of tensile stress allow the occurrence of local structural transformations caused by nonequilibrium state in this zone.

As it was mentioned above, a similar situation is observed for biological membranes under the action of various external factors (metal oxide nanoparticles, stress hormones). In biological membranes considered as liquid crystals, the system-forming bonds are represented by low-energy forces: covalent and hydrogen bonds, hydrophobic and weak electrostatic interactions. They serve as the memory elements and determine also a low shear strength of biological membranes and such notion as membrane "liquidness". It can be stated that homeostatic mechanisms of physical and biological systems in dissipative state are universal.

The concept of homeostatic determinate systems is fundamental for synergetics. It provides deep insight into physical meaning and genesis of the hierarchy of instabilities in self-organizing homeostatic systems, into the nature of interrelations between instabilities and order parameters (Panin, 2008; Panin & Panin, 2004).

Under homeostatic determinate systems we understand such systems where the eventual (actual) result of an action is predicted (determined) via the interaction of signals specific for the given system with its memory elements. Structurally such systems include determinate synthesis, choice of an adequate action program, its outcome, and feedback closed on results-of-action acceptor (fig. 27).

The most complex element of any homeostatic determinate system is the determinate synthesis. Here the dominant motivation, conditional (environmental) and causal (triggering) afferentation interact with the memory elements of the system. This results in decision making and choosing a termodinamic determined action program. Information on the achieved result goes to results-of-action acceptor (feedback), where the anticipated and

actual results are compared. If the goal is not reached, i.e., the actual result does not fit the anticipated one, homeostatic determinate systems switch over to another programs due to changes in the decision made.

Thus, in the expression "homeostatic determinant system" the term "homeostatic" imlies a basic property of the system, its stability, resistance, and the term "determinant" defines the mechanism for achieving this aim and the determinant type of behavior of the system.
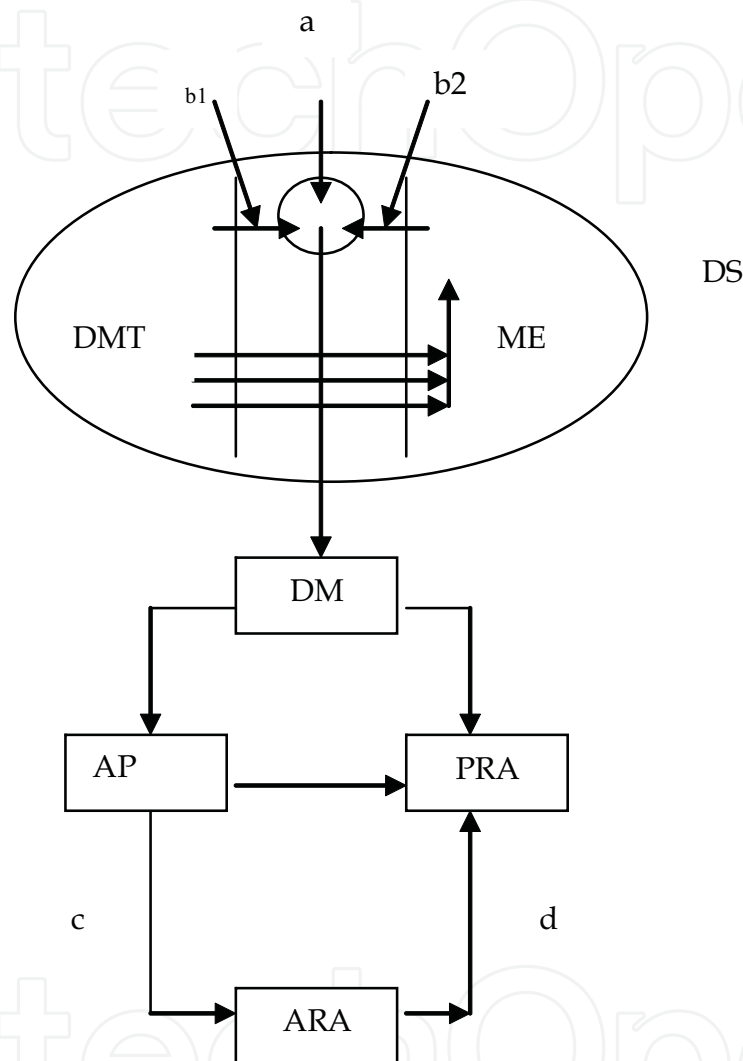

Fig. 27. A schematic diagram of homeostatic determinate system
DMT – dominant motivation: system in a condition of thermodynamic balance; ME – memory elements: metal, covalent and hydrogen bonds, electrostatic and hydrophobic interactions; a — trigger signaling: specific signals able to interact with ME (mechanical load, temperature, pressure, electric discharges, etc.; b_1 and b_2 — circumstantial signaling: additional signaling accompanying the main one, for example, an excited environment; DM — decision making: transition of crystal to a new level of systemic organization; AP — action program: formation of new bonds, which change negenthropy (information) or enthropy; ARA – actual results of action: emergence of a new system in one of energetically allowed state; PRA — predicted result of action: emergence of a new system in the energetically stable state; DS — determinate synthesis, decision-making process; c and d — straight line and feedback

Thermodynamics and Mesomechanics of Nanostructural Transitions
in Biological Membranes as Liquid Cristals
349

Destruction of solid and liquid crystals increases the molar volume.

A dependence of the Gibbs thermodynamic potential $F(\upsilon)$ on the molar volume υ taking into account local zones of different scale stress concentrators is described by the equation:

$$F(\upsilon) = U - TS + p\upsilon - \Sigma\mu_i C_i, \qquad (19)$$

where μ_i – chemical potential, C_i – concentration (fig. 28, Panin & Egorushkin, 2008).

At critical values of molar volume $\upsilon_i = (1,2\ldots6)$, the thermodynamic potential $F(\upsilon)$ has local minima. They reflect local nonequilibrium potentials in the zones of different scale hydrostatic tension. Critical values of υ_i correspond to different levels of homeostasis in a deformable solid:

υ_0 is an equilibrium crystal; the initial level of homeostasis;

υ_1 are the zones of stress microconcentrators where dislocation cores are generated; the next level of homeostasis;

υ_2, υ_3 are the zones of stress meso- and macroconcentrators where local structural-phase transitions with the formation of meso- and macrostripes of local plastic deformation take place; the next levels of homeostasis;

υ_4 corresponds to intersection of curve $F(\upsilon)$ with the abscissa. At a further increase of the local molar volume, changes of the Gibbs thermodynamic potential proceed under the conditions of $F(\upsilon) > 0$, and the system becomes unstable. Various forms of material failure appear; solid crystal starts to behave as a liquid one.

$\upsilon > \upsilon_6$ – the existence of two phases is possible: at $\upsilon = \upsilon_5$ – the vacancy phase atom, at $\upsilon > \upsilon_6$ – different thermodynamic levels of the crystal lattice in a deformable solid, different levels of its homeostasis.
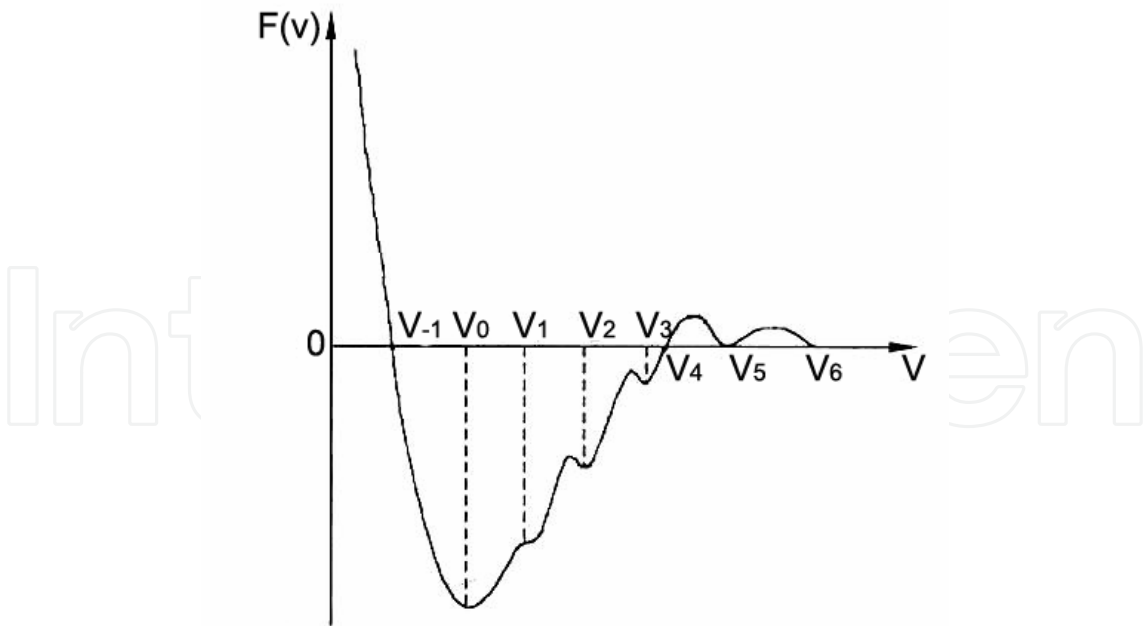

Fig. 28. The dependence of the Gibbs thermodynamic potential F (v) from the molar volume v in the light of local zones of stress concentrators of different scale (Panin & Egorushkin, 2008)

Thus, plastic deformation of solid and liquid heterocrystals in the fields of external action is a multilevel process of their destruction, with the corresponding levels of crystal lattice self-

organization and levels of its homeostasis, i.e., the destruction via different phases of strengthening (self-organization).

Here we see the universal nature of homeostasis of biological and physical systems in dissipative state.

From a physical standpoint, the evolution of material word is based on increasing negentropy, i.e., the degree of orderliness. E. Schrodinger defined it as

$$-S = k \lg (1/D), \tag{20}$$

where $-S$ is the negative entropy, or negentropy; k is the Boltzmann's constant equal to $3.2983 \cdot 10^{-24}$ cal/deg; D is the quantitative measure of disorderliness of atoms in the system, $\lg (1/D)$ is the negative logarithm of D, and $1/D$ is the measure of orderliness. This is the way to estimate negenthropy in liquid and solid crystals.

However, of prime importance for us is that increasing negentropy is always supported by increasing amount of structural information. This can be expressed by the following equation:

$$-S = k \lg(1/D) + \sum p_i \cdot \log p_i \tag{21}$$

where p_i is the probability of individual events in the system. Thus, the informational component in this equation determines an increase of negentropy in the system and is related with acquisition of new properties.

Developing the concept about a correspondence between negentropy and structural information, we can present the following equality:

$$-S = k \lg(1/D) = \sum p_i \cdot \log p_i \tag{22}$$

Hence,

$$\lg (1/D) = (\sum p_i \cdot \log p_i)/k, \text{ and} \tag{23}$$

$$1/D = 10^{(\sum p_i \cdot \log p_i)/k,} \text{ then} \tag{24}$$

$$D = 10^{-(\sum p_i \cdot \log p_i)/k} \text{ or } 1/10^{\sum p_i \cdot \log p_i)/k} \tag{25}$$

Then dependence of Gibbs thermodynamic potential F(υ) on the molar volume υ taking into account local zones of stress concentratotrs is determined by the expression:

$$F (υ) = U - T/10^{(\sum p_i \cdot \log p_i)/k} + pυ - \sum \mu_i C_i, \tag{26}$$

These quantitative interrelations underlie the emergence of new homeostatic determinate systems with new properties in the nature.

The principles of systemic organization of matter based on homeostatic determinate systems, where memory elements are represented by metal, covalent and hydrogen bonds, electrostatic and hydrophobic interactions, have gained wide acceptance in physics and chemistry. The formation of hydrogen molecules from hydrogen atom is a simple example of mechanism self-organization.

The structure of hydrogen atom is very simple: a proton with an electron revolving around it. In the atomic state, hydrogen is a gas with a high level of entropy (low level of negenthropy). Its atoms, colliding with each other, excite electrons, thus making them to

Thermodynamics and Mesomechanics of Nanostructural Transitions
in Biological Membranes as Liquid Cristals
351

occupy different energy levels and sublevels. Such electrons have a large number of degrees of freedom. However, the most probable is the state when electron occupies the lowest energy level (Is). For such a gas, temperature elevation serves as a specific signal interacting with the memory elements (electromagnetic forces). As kinetic energy of the gas increases to a certain value, atoms having electrons at the 1s-level will interact with each other to form hydrogen molecules. Therewith, electrons form a new hybrid wave.

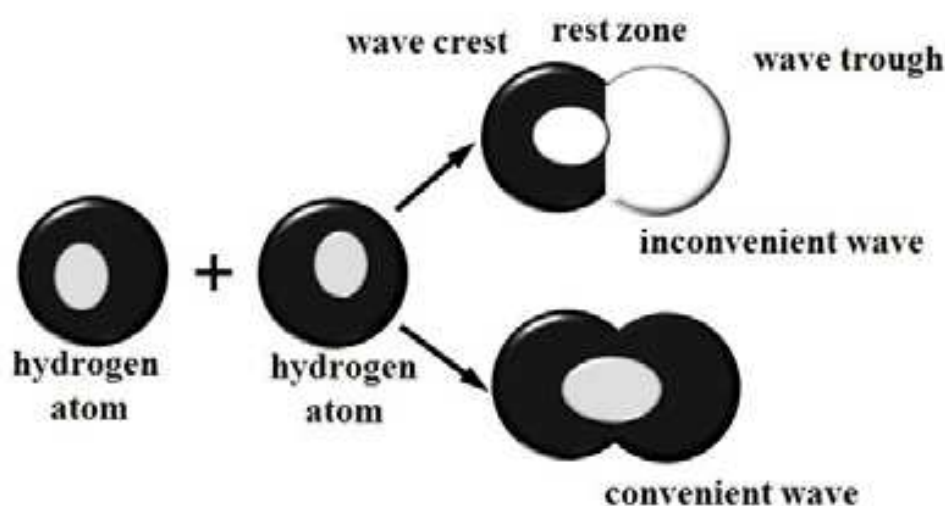Different programs used for the formation of covalent bonds in hydrogen molecules (fig. 29).

Fig. 29. Programs used for the formation of covalent bonds in hydrogen molecules

At the most stable state of such molecules, the gain in energy attains 4 eV. Another essential aspect of this directional process is increasing the amount of information related to electrons. It is described by the Shannon equation:

$$- H = \Sigma p_i \log p_i \qquad (27)$$

In atomic hydrogen, the probability that electron occupies one of allowed energy levels is rather high. A minimum of information is connected with such electrons. When each pair of electrons forms a new hybrid wave, this abruptly decreases the number of degrees of freedom, and their behavior becomes determinate. In a new wave, each electron may stay only in one of two allowed states, which differ in their spin (+1/2 or –1/2). The amount of information connected with such electron increases and depends on the quantity $1/2 \cdot \log 1/2$. For each pair of electrons this will be equal to $\log 1/2$. Multiplying this quantity with the number of hydrogen molecules in the given gas volume gives the total amount of information connected with electrons. This value corresponds to an increase of negentropy upon transition from atomic to molecular hydrogen.

Decomposition of H_2 molecules yielding atomic hydrogen will give rise to an inverse process: decreasing negentropy (structural information) and growing entropy. Similar mechanisms show up also upon destruction of heterocrystals in the fields of external action.

6. Conclusion

Thus, thermodynamics and mesomechanics of nanostructural transitions in biological membranes as liquid crystals resemble structural transitions that occur in solid crystals in

the fields of external action. The distinction is that system-forming binding in biological membranes is represented by covalent and hydrogen bonds, hydrophobic and electrostatic interactions. These are the low-energy bonds. They determine a weak shear strength and such feature as "liquidness" of the membranes. This is very important for functioning of, e.g., erythrocytes that move in the capillary network. Capillary and erythrocyte have comparable sizes, so the movement of erythrocyte is hampered by the frictional force. However, high fluidity of erythrocyte cell membrane makes this process feasible under normal conditions. In extreme states or at pathology related with changes in temperature, blood pH and its salt composition, structural phase transitions are observed in the membranes. There are the smectic A → smectic C, smectic → cholesteric and nematic → isotropic state transitions. In membrane bound proteins, the tangle → α-helix and tangle → β-structure transitions are essential. They alter the membrane properties, in particular their "fluidity".

Structural phase transitions in erythrocyte membranes occur also under the action of stress hormones (cortisol, adrenaline). The active CO and OH groups of the hormones interact with CO and NH groups of the cell membrane proteins and phospholipids to form hydrogen bonds. Large domains form on the cell surface, which comprise structural proteins and local phospholipid environment. Hydrophobic rings of the hormones enhance hydrophobic interactions in the domains. Water dipoles are displaced to adjacent regions and facilitate there the action of stretching hydrostatic forces. This leads to appearance of nanostructural phase boundaries, along which the membrane damage occurs. The plastic deformation meso-stripes with bifurcations are formed. Viscosity of such membranes increases in the region of lipid-lipid and protein-lipid interactions. Such erythrocytes are able to occlude capillaries. In the heart, this may cause diffusion hypoxia and sudden cardiac arrest. Such cases were observed recently in sportsmen during the high-level competitions (Courson, 2007; Montagnana et al., 2008).

Damage of erythrocyte membranes upon interaction with metal oxide nanoparticles follows the same way. Hydrophobic particles of size 5-10 nm penetrate deep into a lipid bilayer. Due to enhancement of hydrophobic interactions, water dipoles are displaced to adjacent regions. Here, the stretching hydrostatic forces lead to the formation of microcracks and meso-stripes of plastic deformation.

In solid crystals, system-forming bonds are represented by strong interactions. This is the metallic bonding, which has a quantum-mechanical nature. Such crystals possess a high shear strength. However, "pumping" of additional energy in the fields of external action causes a local loss of shear strength, which is accompanied by local structural-phase transformations in the crystal lattice.

Biological membranes and solid crystals are the self-organizing systems. In the process of destruction, they pass several levels of self-organization, with the corresponding hierarchy of instabilities. In terms of synergetics, they are the homeostatic determinate systems. In such systems, memory elements are represented by the system-forming bonds: metallic, covalent and hydrogen bonds, hydrophobic and electrostatic interactions. Exerting some effect on these bonds, external factors induce transition of the system to a new level of homeostasis or self-organization, i.e., to thermodynamically steady states. Ultimately, such transitions may result in complete demolition of the system. All that indicates a mechanistic similarity in the behavior of biological membranes and solid crystals.

Thus, the introduction of principles and regularities of physical mesomechanics in biology provides a deep insight into the mechanism interrelating structure and function of biological

membranes, both in the norm and at systemic membrane pathology (upon variation of hormone concentration, temperature, pH, chemical potencial etc.).

It's may to agree with Henri Poincare, who believed that "the true and only aim of science is to discover unity, but not mechanism".

7. References

Attallah, N.A. & Lata, G.F. (1968). Steroid-protein interactions studied by fluorescence quenching. *Biochim Biophys Acta*, Vol. 168. Issue 2, (October 1968) pp. 321-333, ISSN 0005-2795

Courson, R. (2007). Preventing sudden death on the athletic field; the emergency action plan. *Curr. Sports Med.Rep.*, Vol. 6, No. 2, (Apr. 2007) pp. 93-100, ISSN 1537-890X

Dawson, R.M.C.; Elliot D.C.; Elliot W.H. & Jones K.M. (1986). *Data for biochemical research*. Clarendon Press, ISBN is absent, Oxford, United Kingdom.

Kunitsyn, V.G.; Panin, L.E. & Polyakov, L.M. (2001). Anomalous change of viscosity and conductivity in blood plasma lipoproteins in the physiological temperature range. *Int. J. Quantum Chem.*, Vol. 81, (Feb. 2001) pp. 348-369. ISSN 0020-7608

Leto, T.L. & Marchesi V.T., (1984) A structural model of human erythrocyte protein 4.1. *J. Biol. Chem.*, Vol. 259, N. 7. (Apr. 1984) pp. 4603-4608, ISSN 0021-9258

Montagnana, M.; Lippi, G.; Franchini M.; Banfi, G. & Guidi, G.C. (2008). Sudden cardiac death in young athletes. *Intern. Med.*, Vol. 47, No. 15, (Aug. 2008) pp. 1373-1378, ISSN: 0918-2918

Nicolis, G. & Prigogin I. (1979). Self-organization in nonequilibrium systems. *From dissipative structures to orderliness through fluctuation*, Mir, ISBN, Moscow, Russia

Observation on the Soviet/Canada Transpolar Ski Trek (1992). R.J.Shepard, A. Rode (Ed.), Karger, ISBN 3-8055-5410-9, Basel, Switzerland

Ooi, T.; Itsuka, A.; Onari S. et al. (1988). *Biopolymers*, Imanisi Y. (Ed.), Mir, ISBN is absent, Moscow, Russia

Palek, J. & Sahr, K.E. (1992). Mutations of the red blood cell membrane proteins: from clinical evaluation to detection of the underlying genetic defect. *Blood*, Vol. 80, No. 2, (Jul. 1992) pp. 308-330, ISSN 0006-4971

Panin, L.E. (2008). *Determinate systems in physics, chemistry and biology*. Siberian University publishing house, ISBN 978-5-379-00495-8, Novosibirsk, Russia

Panin, V.E.; Dudarev, E.F. & Bushnev, L.S. (1971). Structure and mechanical properties of substitutional solid solutions, *Metallurgy*, ISBN is absent, Moscow.

Panin, V.E. & Egorushkin, V.E. (2008). Nonequilibrium thermodynamics of a deformed solid as a multilevel system. Corpuscular-wave dualism of plastic shear. *Physical Mesomechanics*, Vol. 11, N. 2. (Mar.-Apr. 2008) pp. 9-30, ISSN 1029-9599

Panin, V.E. & Panin, L.E. (2004). Scale levels of homeostasis in a deformable solid. *Physical Mesomechanics*, Vol. 7, No. 4, (Jul.-Aug. 2004) pp. 5-23, ISSN 1029-9599

Panin, L.E. & Panin, V.E. (2007). Effect of the "chessboard" and mass transfer in interfacial media of organic and inorganic nature. *Physical Mesomechanics*, Vol. 10, No. 6, (Dec. 2007) pp. 5-20, ISSN 1029-9599

Sergeev, P.V.; Galenko-Yaroshevskiy, P.A. & Shymanowski, N.L. (1996). *Studies of biochemical pharmacology*, Gogotova, M.V. (Ed.), R.TS. Farmedinfo, ISBN 5-85556-018-X, Moscow, Russia

Shaniavski, A.A. (2007). *Modeling of fatigue cracking of metals. Synergetics for aviation*, Publishing Hause of Scientific-and-Technical Literature, "Monography", ISBN 978-5-94920-058-2, Ufa, Russia

Wu, G.; Hu, G; Cai, J.; Ma, S.; Wang. X.; Chen, G. & Pan, G. (2009). Time-dependent surface adhesive force and morphology of RBC measured by AFM. *Micron*,Vol. 40, Issue 3., (Apr. 2009) pp. 359-364. ISSN 0968-4328
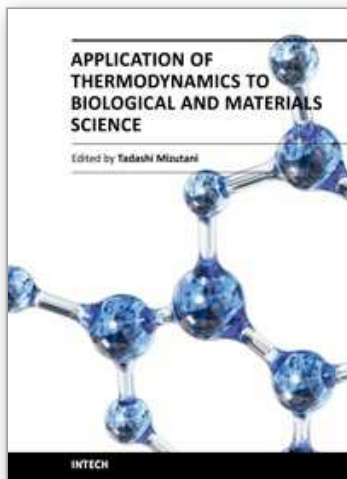
Application of Thermodynamics to Biological and Materials Science

Edited by Prof. Mizutani Tadashi

Progress of thermodynamics has been stimulated by the findings of a variety of fields of science and technology. The principles of thermodynamics are so general that the application is widespread to such fields as solid state physics, chemistry, biology, astronomical science, materials science, and chemical engineering. The contents of this book should be of help to many scientists and engineers.

How to reference

In order to correctly reference this scholarly work, feel free to copy and paste the following:

Lev Panin (2011). Thermodynamics and Mesomechanics of Nanostructural Transitions in Biological Membranes as Liquid Crystals, Application of Thermodynamics to Biological and Materials Science, Prof. Mizutani Tadashi (Ed.), ISBN: 978-953-307-980-6, InTech, Available from:
http://www.intechopen.com/books/application-of-thermodynamics-to-biological-and-materials-science/thermodynamics-and-mesomechanics-of-nanostructural-transitions-in-biological-membranes-as-liquid-cry

INTECH
open science | open minds